AES/AW/06-26

# Modeling sediment storage in a tidal dominated delta, the Fly River, Papua New Guinea

August 2006

Nawien R. Sheombarsing

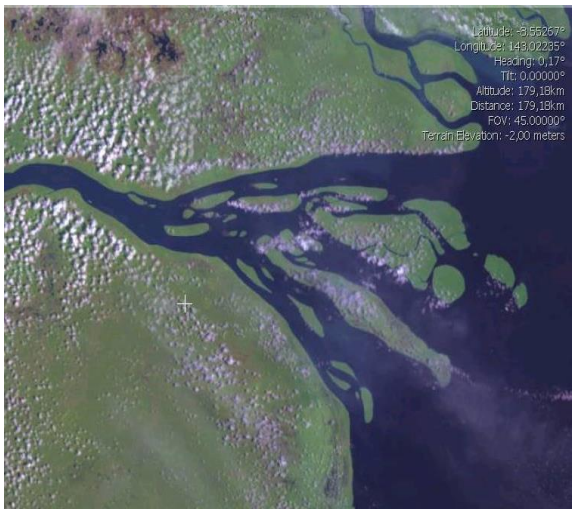


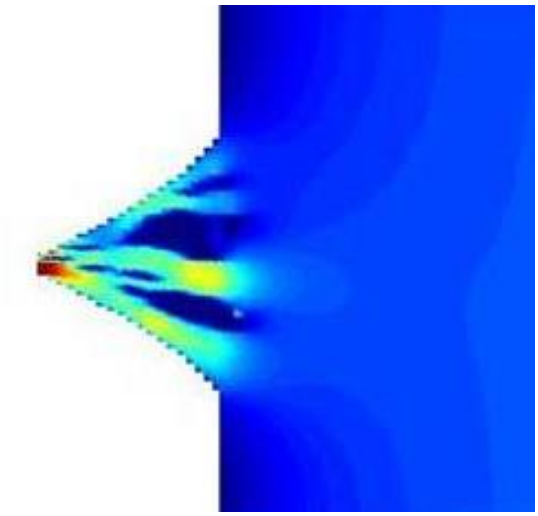

Faculty of Civil Engineering and Geosciences
Department of Geotechnology

Delft University of Technology

| | | |
|---|---|---|
| Title | : | Modeling sediment storage in a tidal dominated delta, the Fly River, Papua New Guinea |
| Author(s) | : | Nawien R. Sheombarsing |
| Date | : | August 2006 |
| Professor | : | Prof. Dr. S.B. Kroonenberg |
| Supervisor(s) | : | Dr.Ir. I. Overeem, Dr. J. Storms, Dr G.J. Weltje |
| TA Report number | : | AES/AW 06-26 |


| | | |
|---|---|---|
| Postal Address | : | Section for Earth Sciences<br>Department of Applied Earth Sciences<br>Delft University of Technology<br>P.O. Box 5028<br>The Netherlands |
| Telephone | : | (31) 15 2785722<br>(31) 15 2781328 (secretary) |
| Telefax | : | (31) 15 2781189 |
| Electronic-mail | : | rishi_1978@yahoo.com |

# PREFACE

This thesis is composed to fulfill the partial requirement for obtaining the degree of Master of Science at the department of Applied Earth Sciences, Faculty of Civil Engineering and Geosciences of the Delft University of Technology. It involves the research project "Modeling sediment storage in a tidal dominated delta, the Fly River, Papua New Guinea". This project falls in the framework of the MARGINS Source-to-Sink project, funded by the US National Science Foundation. This research project has been carried out between December 2005 and August 2006.

The aim of this MSc research project is to model the sediment storage in a tide dominated delta and study its morphological changes due to annual conditions and for peak and low flow conditions. Delft3D is used as process based modeling software to execute the modeling part of this research. It creates the possibility to run several scenarios with different varying conditions such as river discharge and sediment load. During this research knowledge has been gained how the sedimentological depositions evolve within such a tidal deltaic system, though in a general view.

Nawien R. Sheombarsing

# ABSTRACT

Tide dominated deltas are not studied so extensively as river-dominated and wave-dominated deltas. Although, a huge amount of sediments supplied by major rivers, is stored in tide dominated deltas. This suggests that sediment dispersal and deposition in coastal areas are mainly controlled by tidal currents. Long-term stratigraphical numerical models has until now not included the influences of tidal processes properly, although they have high influences. Through modeling of a tide dominated delta, insight will be achieved about the influences of tidal and fluvial processes on sediment transport and deposition in these tide dominated environments. Process based modeling of tide dominated deposits makes it possible to distinguish the controls of tidal depositional processes on the depositional architecture in terms of reservoir properties. Due to the fact that tide-dominated deposits are very heterogeneous, process based modeling of these deposits could support high resolution correlation and delineation of reservoir flow units.

The purpose of this research was to study the process based sedimentation model for tidal influenced deltaic deposits when considering variable sediment load and river discharges. The objective was to model the sediment storage in the tide dominated delta and to study morphological changes in the delta at annual conditions and due to variable river discharge and sediment load.

The research method involves process based modeling with the Delft3D modeling software. Here several scenarios have been executed while varying parameters, which control river and tidal influences. The simulation results were used to study the sedimentation pattern development and morphological changes within a tide dominated delta. This research uses the Fly delta, in Papua New Guinea as case study area, with the focus on the area between the apex and the mouth of the delta.
Depth average velocity and yearly sedimentation rates were used as criteria to select the most suitable scaled sediment load scenario for the simulations.
Bed level study shows that the sedimentation rates varies within the delta, with highest sedimentation in the mid-delta area, and lowest at the channel mouth. Sedimentation rate differs also between the delta channels as well as within the individual channel. Decrease in sediment deposition during low flow conditions was relatively larger, while the high flow conditions causes a smaller increase in sediment deposition. The El Niño extreme low flow scenario shows a predictable result of only sediment deposition at the delta apex, due to low velocity and low river discharge, sediment has not been transported towards downstream area. With tide and without tide scenarios, resulted into small scale differences in sedimentation patterns, based on grainsize characteristics. Other sedimentation differences may occur on local level within specific parts of the delta.

The morphological development shows that changes around a specific island has resulted scouring of the channel bottom at tidal conditions and deposition of coarse grained sediments along the sides of the channel. Further it was distinguished that the highest sand accumulation has been occurred at the upstream part of the island and the highest clay sedimentation at the downstream part of the island. This characterize an important difference between more fluvial-dominated deltas and tide-dominated deltas

The main problem during modeling was related to the scaling of the model according to the Fly delta geometry and flow conditions. This was caused by the Delft3D model limitations, for size and resolution of the model grid.
Overall we conclude that longer-term simulations create the possibility to study the morphological development within the delta in more detail.

# TABLE OF CONTENTS

# 1 INTRODUCTION

## 1.1 General research framework

The morphology and sedimentary processes of tidal-dominated deltas are the less studied as compared to river-dominated and wave-dominated deltas *(Bhattacharya and Walker, 1992, Harris et al., 1993).* Still, 30% of the largest rivers discharge into oceans with a tidal range of 3 m or greater and 60% of the sediment supplied to the ocean by major rivers is deposited in deltas with a tidal range greater than 3 m *(Milliman and Syvitski, 1992; Harris et al., 1993).* It is thus clear that tidal currents play a dominant role in controlling sediment dispersal and deposition in coastal areas.

In this study we work with the numeric tidal delta module of DELFT3D and we selected the Fly River delta as a case study. The Fly River delta is a classic tide-dominated system, used as the end-member example in the delta classification scheme created by Galloway (1975).

Tidal processes are until now not considered seriously in long-term stratigraphical numerical models, although they have big influences. Modelling of a tide dominated delta will give insight about the influence of tide and fluvial processes on sediment transport and accumulation in such an environment.

## 1.2 Research objective

The purpose of this research work is to study a process based sedimentation model for tidal influenced deltaic deposits with focus on variable sediment load and river discharge values. The objectives are as follows:

1) Model the sediment storage in the tide dominated deltaic environment
2) Investigate morphological changes in the tide dominated delta due to varying conditions such as varying sediment load and river discharge, i.e under low/peak flow conditions, and with tides and without tides.

## 1.3 Relevance of this research for oil reservoir geology

Process based modelling of sedimentary environments could support high resolution correlation and delineation of reservoir flow units. Geometry of reservoir sands and stacking pattern of channels and bars as well as internal heterogeneities within the individual bars/ channels are all affected by changes in the sedimentary processes. Process based modelling makes it possible to quantify the controls of tidal depositional processes on the depositional architecture in terms of effective reservoir properties as grain size and net-gross ratio and even porosity and permeability.

Tide dominated reservoirs host major hydrocarbon accumulations in the world such as in Venezuela, Columbia, Equador, Canada and offshore Norway. Characterization and modeling of tidal reservoirs is not easy due to complex sedimentary heterogeneity of these deposits varying from small to large scale. The complexity of these tidal deposits forms a main concern of geologists. To

improve the understanding of this type of deposits and to achieve optimal production within these areas geological modeling is important.

## 1.4 Research method

Our research method involves process based modeling by using the physics based Delft3D modeling software developed at the WL/Delft Hydraulics. Delft3D links a number of numerical modules to simulate hydrodynamic flow, which can incorporate tides and waves and the transport of sediment and morphological changes. The model is used to run several selected scenarios varying key controlling factors, focusing on river influence and tidal influence. The simulation results will provide ideas about how the sedimentation patterns evolve within a tide dominated delta and which morphological changes have occurred.
For this research the Fly delta, Papua New Guinea, is used as case study area. This research will focus on the Fly river, especially from the apex of the Fly delta, to the mouth of the delta. The measurements and geometrical values of the Fly delta are used as a guide for setting the scenarios and running the simulations.

## 1.5 Research Question and Hypothesis

The main research questions are:

How much of the sediment is stored in the tide dominated delta?

What are the influences of the annual sediment load and discharges? Which influences do peak / low flow events have on the morphological development within a tide dominated delta?

## 1.6 Report outline

Chapter 2 introduces concepts and definitions that are used in the description of tide dominated deltas and introduce the Fly River and Delta. Chapter 3 describes the observational data which is used as input for the modeling experiments. In chapter 4, the Delft 3D Model concepts are discussed. Chapter 5 consists of an overview of the Delft3D Model Experimental set up. The results are presented in chapter 6. Finally, discussion, conclusion and recommendations for future research are provided in chapter 7.

# 2. LITERATURE STUDY

## 2.1 Deltas

### 2.1.1 Introduction

Deltas are sedimentary bodies that formed at the mouth of a river which are building outwards into a lacustrine or marine basin through time *(Nichols, 1999).* Delta environments have large amounts of net accumulation because sediments are supplied more rapidly than they may be redistributed in the basin. Their preservation potential is high if the area is a region of overall subsidence. Delta areas are very sensitive to changes in sea level caused by uplift and subsidence of the land or changes in the absolute level of the sea. This causes migration of the river mouth and progradation of the delta lobe into the receiving basin, these processes resulted into partly preservation of deposits in depth. The considerable accumulations of sediment, together with the presence of large amounts of vegetation imply that ancient deltaic deposits are important as source and reservoir rock for hydrocarbons.

### 2.1.2 Morphological characteristics

Deltas consist of a subaerial and a subaqueous part. The subaerial part or delta plain is divided into an upper delta plain (fluvial dominated) and a lower delta plain (marine influenced) part *(see Fig. 2.1)*.

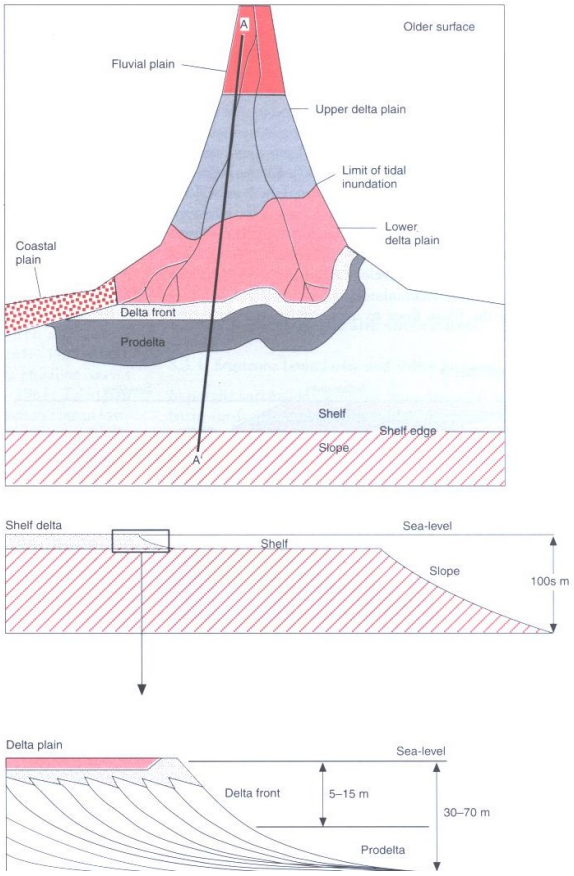


*Figure 2.1 Delta environments (Reynolds, 1996)*

The upper delta plain is an extensive floodplain downstream of the delta apex often with a number of active channels. The lower delta plain consists of a coastal area crossed by a network of active and abandoned channels which may be separated by either vegetated or shallow water areas, called interdistributary bays. The subaqueous part includes the delta front and prodelta area *(see Fig. 2.1).* The delta front area occurs seawards from the delta plain. It consists of the shoreline and the deltaic part below sea-level, the so-called mouthbar area, with seaward dipping deltaic sediments, the so-called delta slope. Finally, the prodelta area is located offshore, consisting of sediments which have been transported farthest seawards *(Fig. 2.1).*

### 2.1.3 Delta forming processes

Deltas are influenced by several factors; supply controls like river discharge and sediment characteristics, marine controls like the relative importance of waves and tides, and basin controls like bathymetry and subsidence. Galloway (1975) made a classification of the deltas in terms of processes considering the relative importance of river, waves and tidal processes *(Fig. 2.2).*

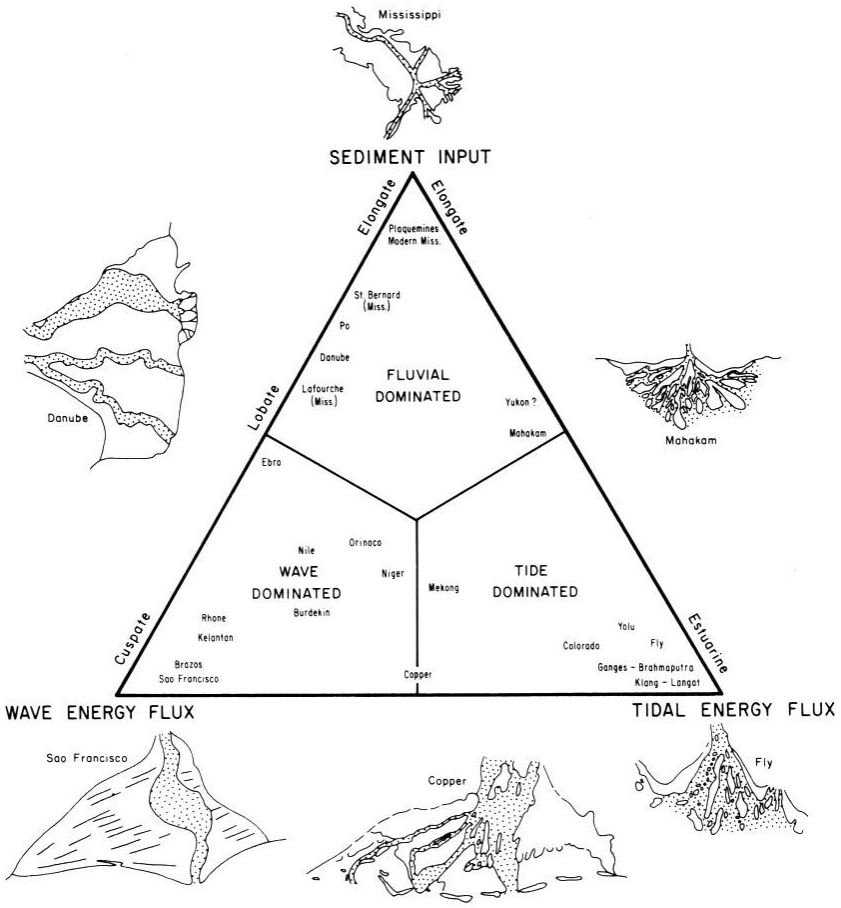


*Figure 2.2 Morphological classification of delta systems (Galloway et al., 1983)*

The three different delta end-members as given in Galloways (1975) classification are: river-dominated deltas, tide-dominated deltas and wave-dominated deltas. The focus of this study is on the Fly delta in Papua New Guinea, which is a pronouncedly tide-dominated delta.

Sedimentation in deltaic areas is mainly influenced by:

1) The ratio of bedload to suspended load and its impact on delta characteristics and facies patterns *(Elliot et al., 1986)*
2) River discharge fluctuations and also its timing in relation to fluctuation in basin energy regime *(Elliot et al., 1986)*

These influences exist also for the Fly delta area, due to the seasonal variations and peak and low flow events. Some of these factors are further investigated in this study.

### 2.1.4 Delta deposition

Typically, deltas are fed by rivers in a low gradient setting nearing the coastal plains, and consequently deltas often have relatively fine-grained deposits, because coarser bedload sediments have been deposited by the river in the upland area before reaching the delta. The grain size range of delta deposits varies from fine sand, very fine sand to silt and clay. The coarsest sediments are deposited in the fluvial channels, where the flow is strong enough to transport and deposit bedload material. The depositional patterns of sediments in the delta mouth area depend on the type and degree of mixing at the distributary mouth and decrease of flow velocity. At the river mouth the river water enters the marine basin causing a mixing process which depends on the water velocity, the density differences between the two water masses and the bed friction. The velocity of the river water is directly related to the channel dimensions and the amount of discharge and typically is less than 1 m/s. The bed friction is related

to the depth as well as on the sediment roughness at the channel mouth, where gentle bathymetry causes increased bed friction and a wider spreading of the delta plume. In most cases the river water has a lower density than the saline seawater; it will form together with its suspended sediment a laterally spreading, buoyant plume floating on top of the marine water, called hypopycnal flow *(see Fig. 2.3).* The mixing processes which occur at the lower boundary of the sediment plume causes flocculation and increased settling of suspended clay. A saltwater wedge beneath prograding river water is formed, and flow separation at the channel mouth occurred. This causes rapid and efficient deposition of bedload sediment as a coarsening upward channel or distributary mouthbar *(see Fig. 2.3).*

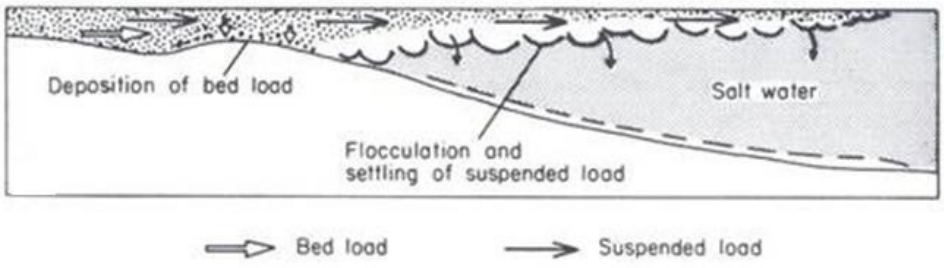


*Figure 2.3 Hypopycnal flow (Galloway et al., 1983)*

Over many years to centuries a delta advances into a marine basin. During progradation of the delta, extension of the river channel occurs over the delta front and mouthbar area. This results into the typical coarsening upwards sedimentation pattern of deltaic deposits.

## 2.1.5 Delta types

### 2.1.5.1 Tide-dominated deltas

In this study we focus on the Fly delta, which is a tide-dominated delta system. Tide-dominated deltas occur in areas where wave action is limited and tidal ranges are generally in excess, generating strong tidal currents. Tide-dominated deltas have characteristic distributary channels with a broad, open or funnel-shaped mouth and narrow sinuous upper reaches. Bedload deposition in the channel mouth and a dominant upwards tidal sediment transport causes filling of distributaries and seaward thickening and widening sand lenses *(Galloway, 1983).* These channel fill deposits are composed of multiple superimposed, and variable preserved, fining-up depositional units. The sediments which are transported by river flow towards the distributary mouths are rapidly reworked by the tidal currents due to bi-directional sediment transport along ebb- and flood dominated pathways into series of linear tidal bars within the distributary mouth and further seawards *(Fig. 2.4, Elliot et al., 1986)*. These linear tidal bars are perpendicular to the shoreline and may separate by finer grained silts and clays. During seawards progradation of the delta, former lineair tidal bars are exposed above sea level and they become colonized by vegetation to form linear tidal islands. The vegetation has a stabilizing effect and so influences channel behavior *(Bearman, 1989).* These tidal islands have a length up to several kilometers, widthness around hundred meters and heights up to 20 m.

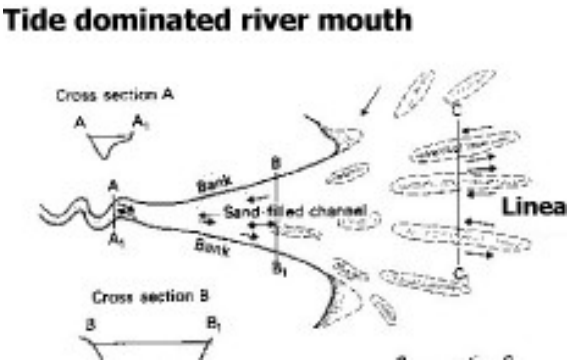


*Figure 2.4 Tide dominated funnel shaped distributary channel with linear tidal bars (Elliot et al., 1986)*

The distributary channels may show lateral migration patterns, which suggest that the sandbody geometry is a function of channel size, form and channel lateral migration pattern *(Fig.2.4; Elliot et al., 1986).*

The two other types of deltas are briefly in the following parts and are not considered further in this study.

#### 2.1.5.2 River dominated deltas

These types of deltas are mainly dominated by fluvial processes of transport and sedimentation. Here the effects of tides and waves are low. The deposits of river dominated deltas consist of channel and overbank deposits *(Nichols, 1999).*

#### 2.1.5.3 Wave dominated deltas

Here waves dominated by strong winds disturb the top few meters of the water column and have the capacity to rework and redistribute any sediment deposited in shallow water. The wave dominated deltaic deposits are well developed mouth bar and beach sediments, which occur as elongated coarse sediment bodies more then less perpendicular to the orientation of the delta river channel *(Nichols, 1999).*

## 2.2 The Fly River and Fly Delta

### 2.2.1 The Fly River basin

The Fly River basin is located on the island of Papua New Guinea-Irian Jaya, which is the northern extension of the Australian continental plate, forming a continent-island arc collision boundary *(see Fig 2.5; Harris et al., 1993).*

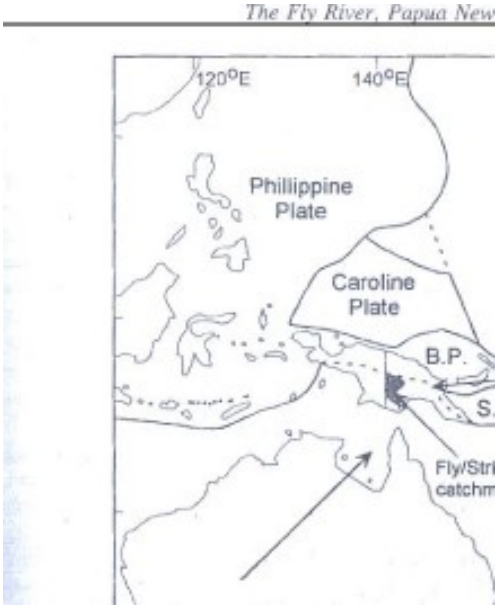


*Figure 2.5 Plate tectonic framework of the Fly River catchment in Papua New Guinea (Dietrich et al., 1999)*

During the early Tertiary time New Guinea and the deep ocean floor to the north of it moved rapidly northward. An island arc, with a north-dipping subduction zone, converged with New Guinea during Late Cretaceous and Early Tertiary, and the Caroline Sea plate opened north of the arc *(Fig 2.5).* The collision of this arc with New Guinea in the Miocene time initiated the rise of the mountains of New Guinea and sedimentation in the foreland basin to the south of them *(Hamilton et al., 1979).* This collision has caused the subduction zone to change its polarity in the Late Tertiary from an original northward dip beneath the island arc, to

southward beneath the New Guinea subcontinent as enlarged by the addition to it of the island arc and related materials (*Johnson, 1976).* The middle Oligocene collision of the northern carbonate shelf margin of the Australian craton with a subduction system resulted in emplacement of a thrust mass and formation of a foreland basin *(Fig. 2.5)*. This caused a broad flexture of the margin; as the northerly migration of the plate pushed into a tropical climate, an extensive carbonate platform formed *(Dietrich et al., 1999)*. Subduction of the northward-migrating Solomon Sea Plate under the South Bismarck Sea Plate and beneath the Pacific plate has taken place *(Fig. 2.5)*. These events cause the occurrences of large volcanic activity in that region *(Hamilton et al., 1979).*
During the late Pliocene and Quaternary, sediment derived from the mountains filled in the foreland basin. Due to continued tectonic activity, these buried sediments were subsequently again uplifted and incised. As such the Fly River basin is located in one of the few modern examples of a developing foreland basin. The Fly River system consist of three major tributaries: the Ok Tedi, Fly and Strickland Rivers, all of which originate in the steep, rapidly uplifting Southern Fold mountains where the peaks reach up to 4000 m in elevation *(see Fig. 2.6; Dietrich et al., 1999).*

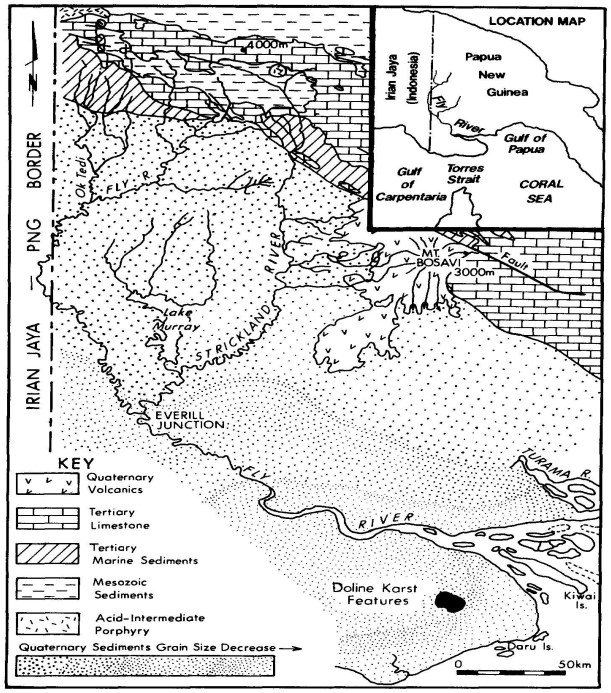


*Figure 2.6 Location map Fly River (Harris et al., 1993)*

The tectonic setting of the Fly River system impacts its sedimentation and transport characteristics. The total drainage area of the Fly River is 76,000 km$^2$ *(Harris et al., 1993)*. The mountains and the tropical climate cause orographic precipitation and thus high rainfall rates. The measured rainfall in the coastal area of the Fly river is 2000 mm/year *(Harris et al., 1993)* and in the highlands it varies between 10000 – 13000 mm/year *(Wolanski et al., 1995a).* In 1997, which

was an El Niño year, a significant drought occurred in the Fly River area, causing a reduction in river flow to approximately 1000 $m^3$/s. The active mountain setting also causes the steep upland topography, which is unstable and prone to massive landsliding supplying high sediment loads to the river system. The steep gradient terrain rapidly declines when entering the adjacent basin. The change in elevation in the Fly River from Upper Fly and Ok Tedi River junction to sea level is only 20 m along an 800 km meandering river valley *(Fig. 2.6).* The active floodplain area is limited to a 10 -15 km wide channel belt with lakes on either side of the active meandering channels *(Dietrich et al., 1999).* These processes result in high sediment loads in the Fly basin *(Dietrich et al., 1999).* Most of the drainage basin of the Fly is relatively unaffected by human activity. However, the Fly River sediment load discharge is presently influenced by mining activities and deforestation *(Harris et al., 1993).*The combined steep upland topography and tropical rainfall rates causes the Fly River to be the 17$^{th}$ largest river in the world in terms of sediment discharge. Modern sediment discharge estimates amount to 115 mln tonnes/year for the Fly river *(Syvitski, 2005)*

### 2.2.2 The Fly River delta

The Fly delta was used as the end-member example in the delta classification system created by Galloway (1975), because the Fly River delta is a classic example of a tide-dominated delta with a funnel shaped mouth and three main distributaries which are separated by elongated vegetated islands *(Fig. 2.7)*. The Fly delta is macro tidal (tidal range > 4m) with a strong semidiurnal asymmetry and a marked neap-spring tidal cycle with a time scale of 14 days. The semidiurnal characteristic suggests that the daily ebb and flood cycle has a time scale of 6 hours. Local tides range from about 3.5 m at the mouth to 5 m at the apex *(Baker et al., 1995)*. Bathymetric and remote sensed imaginary has indicated that there was hardly any change in the areas of the islands and distributaries in the last 50 years *(Baker et al., 1995).* The Fly delta area has depth values often smaller than 10 m; the mean depth is 8 m *(Harris et al., 1993).* It has a progradation rate of 6 m/year and has extended its area 40-50 km since the postglacial transgression has ended locally *(Harris et al., 2004).* The change from transgression to progradation consisted of stages of vertical aggradation and stacking of distributary channels.

The three main distributary channels of the Fly delta are *(Fig. 2.7)*:

1) Southern channel
2) Northern channel
3) Far northern channel

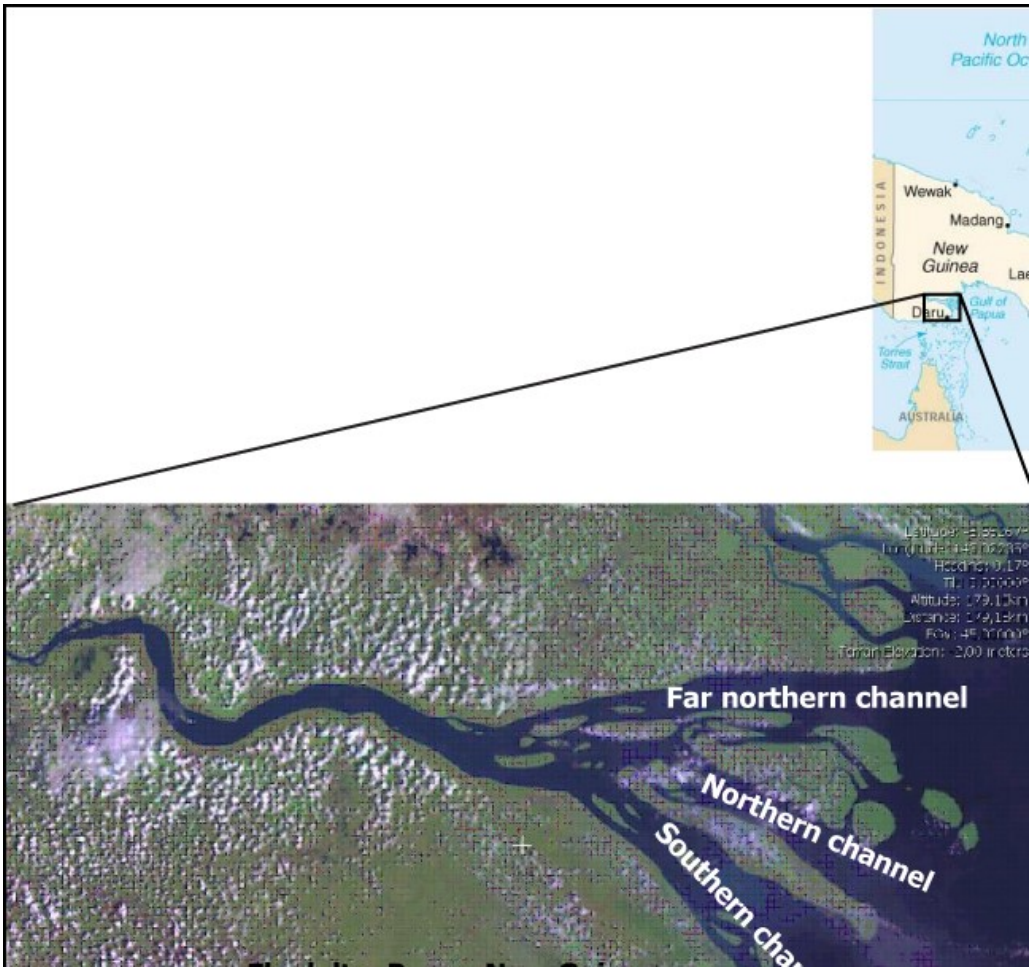


*Figure 2.7 Location map of the Fly delta and the three main distributary channels*

The depth of the distributary channels can be up to approximately 12 m. The main sediment export occurs through the Southern channel (60- 80%). The Far Northern channel is abandoned at present and experiencing widespread erosion by tidal currents *(Dalrymple et al., 2003).*

Tidal currents have major influence on transport and deposition of sandy sediments within the Fly delta. The strong tidal currents control sedimentary structures and geomorphology such as linear tidal bars and funnel shape of the delta *(Harris et al., 1993)*. Apart from the tidal currents there is a strongly seasonally controlled influence of surface waves. Strong surface waves are generated by Southeasterly trade wind (from March to November) and together with tidal currents, they rework muds and sands on the delta front and blow out fine grained sediments into suspension. During the North West monsoon (from December to March) the surface waves are less active. This period of relative quiescence causes the deposition of mud drapes, resulting in seasonal bioturbated sand-mud interbeds. During the summer monsoon the wind blew from the North West. The Fly delta deposits are mud dominated; because the

river flows along a low gradient axis to the fore land basin and medium to fine sediments are deposited in the inland area before reaching the sea.

The Fly delta is divided into the following depositional subenvironments:

1) Delta plain consisting of islands and distributary channels
2) Distributary mouthbars
3) Delta front and Prodelta

1) Delta plain: Islands and Distributary channels

The small islands or tidal bars may contain 50 % or more mud and display lateral accretion bedding. Lateral erosion and accretion of these islands those place several times, causes a shore line migration rate up to 37 m /year *(Harris et al., 1993)*. Most of the tidal bars have a length between 2-8 km and a width range of 0.5-4 km as measured from satellite image data. The length-width relations for these tidal bars are given below in *Fig. 2.8.*

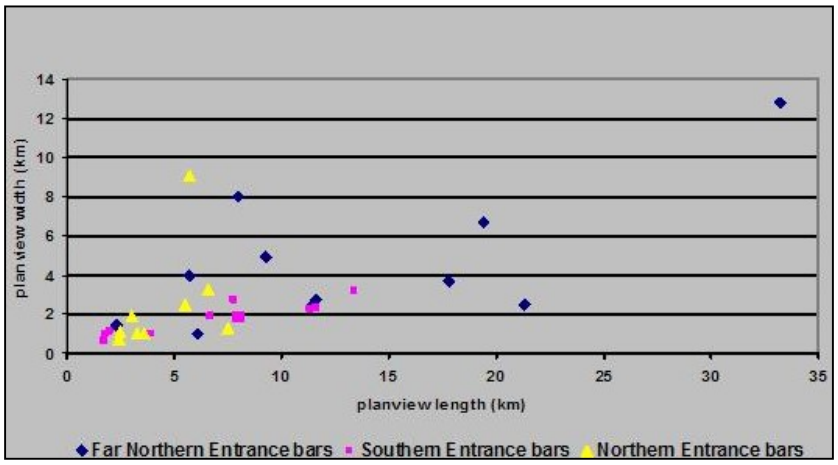


*Figure 2.8 Length-width relation tidal bars Fly delta*

These tidal bars consist of a large amount of mangrove vegetation which has a stabilization effect. Their cohesive mud and root network produce a stratigraphic unit that can be resistant to erosion and form steep banks *(see Fig. 2.9).*

*Figure 2.9 Pre-existing channelized bars, colonized with mangroves*

The distributary channels are characterized by strong tidal currents and high suspended sediment concentrations. The bottom of these distributary channels consist of a thin layer of fine to very fine, cross-bedded sand and mud pebble conglomerates *(Baker et al., 1995).* On top of this, fluid mud deposition occurs, which are formed in the channel bottoms after a spring tide. The locally presence of tidal rhythmites (heterolithic deposits) within the channel indicates a tidally origin.

2) Distributary mouth bars

These are series of elongated tidal bars in the mouthbar area of the delta plain. They could extend up to 15-20 km offshore and have a widthness of 1-6 km *(Dalrymple et al., 2003)*. The distributary mouth bars consist of fine sands in lateral accretion bedding setting and crossbedded coarse sands *(see stratigraphic column Fig. 2.10).* Lateral erosion and accretion of these islands took place several times and causes a shore line migration up to 37 m/year *(Harris et al., 1993)*.

3 Delta front and Prodelta

The delta front and prodelta area is characterize by a broad (ca. 10 km wide), low relief area defined by the 10 m isobath that extends seaward and terminates at a waterdepth of approximately 40-50 m, 40 km offshore, with a slope of $0.0025^0$ *(Dalrymple et al., 2003)*. Delta front and prodelta facies are heterolithic and they consist millimetre to decimetre thick sand/mud alternations *(see stratigraphic column Fig. 2.10).* The delta front deposits occur at depth from 5 – 17 m. They consist of laminated mud-sand deposits. Prodelta deposits occur below the delta front deposits from 17 m to 45 m. The prodelta deposits consist

of massively bedded muds *(see stratigraphic column Fig. 2.10).* The prodelta slope is located between 10 and 30 m isobaths of the Fly River estuary *(Harris et al., 1993)*.

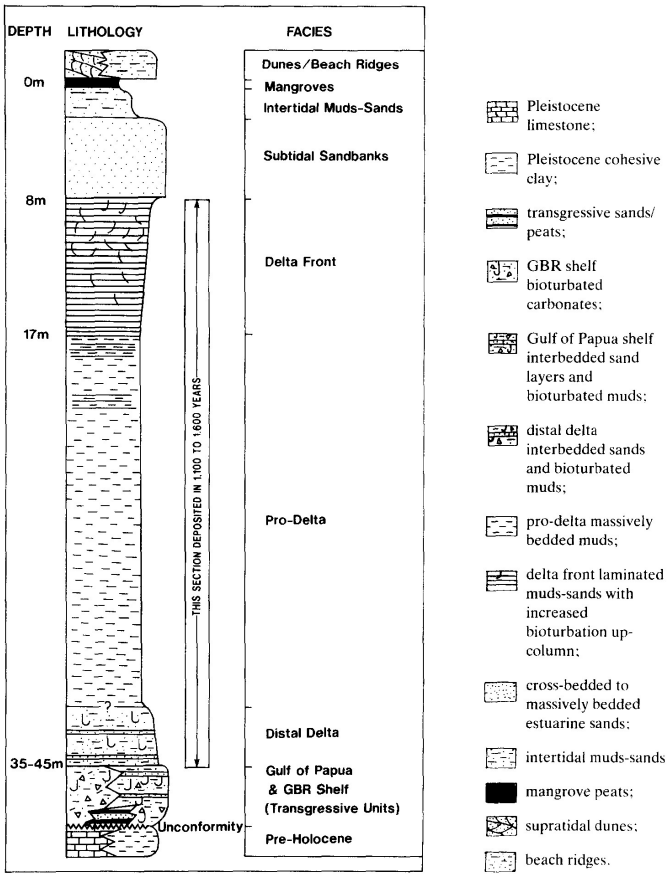


*Figure 2.10 Stratigraphic column Fly delta (Harris et al., 1991)*

Above a stratigraphic section is showing the different sedimentary environments and their facies characteristics, deposit during the offshore progradation of the Fly delta across the shelf. The lithologies are also defined in this figure *(see stratigraphic column Fig. 2.10).* The facies occurrences in the delta front, pro-delta and distal delta area are shown as well as the underlying Gulf of Papua and pre-holocene sediments together with their depth interval. The general stratigraphical facies pattern of the Fly delta consist of sandy channel sands, overlain by thinly bedded and thinly laminated heterolithic (sand and mud) sediments that become finer upward into mangrove muds.

Vibracore data analyses study of Walsh, 2004 identifies four stratigraphic facies within the Fly delta area. These analyses suggest that a common stratigraphy is contained in the prograding mangrove bank deposits. The identified stratigraphic facies were:

1) Supratidal to high tidal muds
2) Mid-tidal sandy muds
3) Low-tidal sand and mud
4) Subtidal channel sands

Supratidal to high tidal muds are typically muddy, homogeneous and contains physical structures as laminations and bedding, which probably indicates high rates of sediment accumulation. Their cohesiveness and presence of abundant roots prevents them against erosion. Mid-tidal and low –tidal sediments are thinly laminated, but could also contain thick laminated deposits from fluid-mud transport. The Subtidal channel sands have thin and thick mud and sand laminations, but are mainly identified by thick sand beds *(Walsh et al., 2004).* The highest sediment accumulation rates as resulted from the vibracore analyses are on accreting banks in the mid-tidal zone, and lower sediment accumulation rates occur below and above this area *(Walsh et al., 2004)*.

## 2.3 The Fly river delta as a reservoir analogue

The tide dominated Fly delta system could potentially be used as a reservoir analogue for oil reservoirs occurring in ancient sedimentary basins with similar depositional environment conditions. A typical modern analogue as the Fly delta can be studied to get in-depth knowledge of the existing depositional processes and characteristics in such a type of environment in order to understand and improve its hydrocarbon behavior. The sand body geometry in modern analogues gives insight on the sandstone geometry in reservoirs.

The hydrocarbon potential of the Fly delta varies due to the high mud content. The best reservoir facies are present in the mouth bar area, because of their relatively great thickness (5-10 m), large lateral extent, both parallel and perpendicular to the coast (many tens of km and perhaps > 10 km respectively) and relative few mud baffles or barriers. Another good reservoir facies accumulation are the channel floor lags, but they are generally thin in the Fly delta and may be of limited lateral extent because of their restriction to areas of local erosion. The lag produced during the abandonment phase of a distributary is potentially more widespread, but the carbonate cementation may be a problem because of the incorporated shell material. The abundance and lateral continuity of mud layers in the heterolithic deposits of tidal bars and pointbars, within the distributary channels resulted in a poor reservoir potential for them.

The C&C reservoirs digital analogues data base for clastic reservoirs was used to identify tide-influenced reservoirs (www.ccreservoirs.com). Their classification indicates that from their own listed 600 clastic reservoirs, 58 reservoirs occur in deltaic environments and from this 9 exist in tide dominated environments (www.ccreservoirs.com).
A number of oilfields in tide-dominated environments for which the Fly delta can act as a reservoir analogue are listed below in *Table 1* together with their relevant producing reservoir interval and age.

| Nr | Field name | Country | Producing reservoir formation | Producing reservoir age |
|---|---|---|---|---|
| 1 | Halten Terrace | Norway | Tilje | Jurassic |
| 2 | Gullfaks | Norway | Cook | Jurassic |
| 3 | Khalda | Egypt | Lower Bahariya | Cretaceous |
| 4 | Meleiha | Egypt | Upper Bahariya | Cretaceous |
| 5 | Duri | Indonesia | Sihapas | Tertiary |
| 6 | Minas | Indonesia | Sihapas | Tertiary |
| 7 | Sacha | Ecuador | Hollin/Napo | Cretaceous |
| 8 | Lagunillas | Venezuela | Misoa | Tertiary |
| 9 | Boscan | Venezuela | Misoa | Tertiary |

*Table 1 Tide influenced hydrocarbon reservoirs (www.ccreservoirs.com)*

The geological characteristics of these tide-dominated reservoirs show similarity with the Fly delta. Heterolithic sandstones are dominant lithofacies of reservoirs existing in tide dominated deltaic environments. Martinus et al., (2005) describe the reservoir deposits in the Halten Terrace reservoirs to consist of lateral shale and siltstone layers with intercalated thin, clean sandstone layers. The reservoir description of these heterolithic deposits are challenging because they consist of marginal reservoir layers with low recovery factors. Often, it remains difficult to recognize and differentiate the different facies types from one another and identify the reservoir and non-reservoir layers. Often the reservoirs are being interpreted to be tidally influenced by the presence of bi-directional cross beds, flaser bedding and abundant clay drapes. Consistingly case-studies of the reservoirs listed in *Table 1* indicate that the distributary mouthbar and tidal channels are identified as the most important reservoir units (Martinus et al., 2005; Gupta et al., 2001; *(Johansen et al., 2003; Toha et al., 2003; Shanmugam et al., 2000; Ambrose et al., 1997).* The mudlayer occurrence and its thickness, extent and frequency influences prediction of permeability and reservoir behaviour to a large extend. Some of these reservoirs, e.g. the Norwegian Cook-3 Formation and the top sandstone units in the Indonesian Duri Formation, occur in an incised valley setting, which is not the case for the present-day, Late-Holocene Fly delta. Other examples may be more reminiscent to the Fly delta, e.g. the Cook 1 and 2 Formations in the Gullfaks field, or the Minas Oilfield in Indonesia

# 3. OBSERVATIONAL DATA FOR MODELING

## 3.1 Introduction

This chapter includes an overview of the observational data, which has been collected for this study of the Fly delta area. The data has been extracted from literature study and only the data applicable for the Delft-3D modeling are discussed here.

Several data sets on the Fly river and delta have been published *(Harris et al., 1993; Walsh et al., 2004; Harris et al., 2004; Dietrich et al., 1999; Wolanski et al., 1995; Dalrymple et al., 2003).* The data include bathymetry, river discharge and sediment load measurements, grain sizes of sediment in transport and depositional units, geometrical data of the channels, tidal measurements, sedimentation rates and wave measurements.

## 3.2 Bathymetry

The bathymetry is a key parameter for modeling the sediment transport and morphological characteristics in the tide dominated Fly delta environment. An initial bathymetric grid is required to start the model simulations. A full digital bathymetric dataset was not available, therefore it was decided to use a schematized bathymetric grid based on the information from the listed studies. The data were generalized from studies done by Harris et al., 1993; Harris et al., 2004; Baker et al., 1995; Wolanski et al., 1997 and Dalrymple et al., 2003. High resolution seismic data from the study of Harris et al., 1993, resulted in knowledge of bathymetric characteristics across delta front and prodelta area. Bathymetric data has been collected in a study of Baker et al., 1995 from echosounding profiles produced by a Raytheon precision depth recorder, which was corrected for tidal elevation and reduced to lowest astronomical tide chart datum. Wolanski et al., 1997 obtained a bathymetric chart from Snowy Mountain Engineering Corporation, Australia and surveyed approximately 20 cross-sections and a approximately 50 single point measurements of depth. The combined maps of these bathymetric surveys show that water depths in the estuary are generally ~8m. Mangrove islands are generally grown to 1-2 m above water level. The channels seldom exceed 12 m water depth and subtidal shallow bars are much shallower. The 5 and 10 m isobaths are located within 20 km from the most seaward edges of the mangrove islands. A steeper prodelta slope is located between the 10 m and 30 m isobaths within 25 km from the delta front. Subsequently the prodelta slopes gradually, to 50 m water depth.

## 3.3 River discharge

River discharge is a measure for the amount of water flowing through the river in a certain time interval. Delft3D requires an input for the fluvial system as a boundary condition. The river discharge is related with the morphological characteristics of the river/delta area. The river discharge dynamics control the width and depth of the channel and flow velocity. This is expressed as follows:

$Q=w\times d\times v$, where (3.1)

Q = discharge ($m^3/s$)
w = width (m)
d = depth (m)
v = velocity (m/s)

The Fly river mean annual discharge at the apex of the delta is estimated to be ~7000 $m^3/s$. This river discharge value is an extrapolation of average monthly river discharges, based on 10-years measurements at Kuambit in the upper part of the Fly River between 1978 and 1988 by Snowy Mountain Engineering Corporation, Australia (Harris et al., 2004). The highest average discharge occurs in June and the lowest discharge occurs in November. The discharge is controlled by rainfall in the mountainous areas. The Fly River contributes about 2500 $m^3/s$ and the Strickland River about 3000 $m^3/s$ at Everill Junction (Harris et al., 2004). The combined Fly River continues for another 300 km downstream and the total mean annual discharge at the delta apex increases to the estimated 7000 $m^3/s$. Syvitski et al., 2005 use a water balance model combining drainage basin characteristics and climate stations to estimate the seasonal Fly river discharge. Seasonal discharges range from ~3200 to 5600 $m^3/s$, with an annual average discharge of ~4400 $m^3/s$ *(see Fig. 3.1)*. The seasonal discharge varies within a range of 25%.

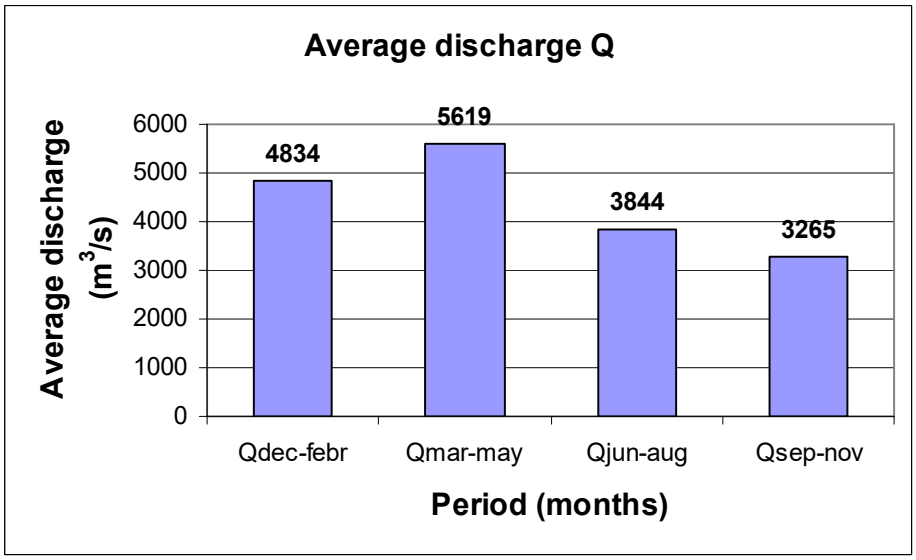


*Figure 3.1 Predicted seasonal river discharge (modified after Syvitski et al., 2005).*

Satellite images over a 5 year time period (2001-2006) have been collected of the Fly delta area in order to investigate changes river flow behavior during high and low discharge periods. The satellite images were collected from the online Terra database ( http://rapidfire.sci.gsfc.nasa.gov). They have a resolution of 250 m or 500 m depending on the date of collection. The images were chosen based on the two different seasons in the Fly delta. Only a limited number of clear images is available due to the frequent presence of clouds. A few characteristic snapshot images from 2001 and 2006 are shown below during periods of high and low rainfall *(see Fig. 3.2)*.

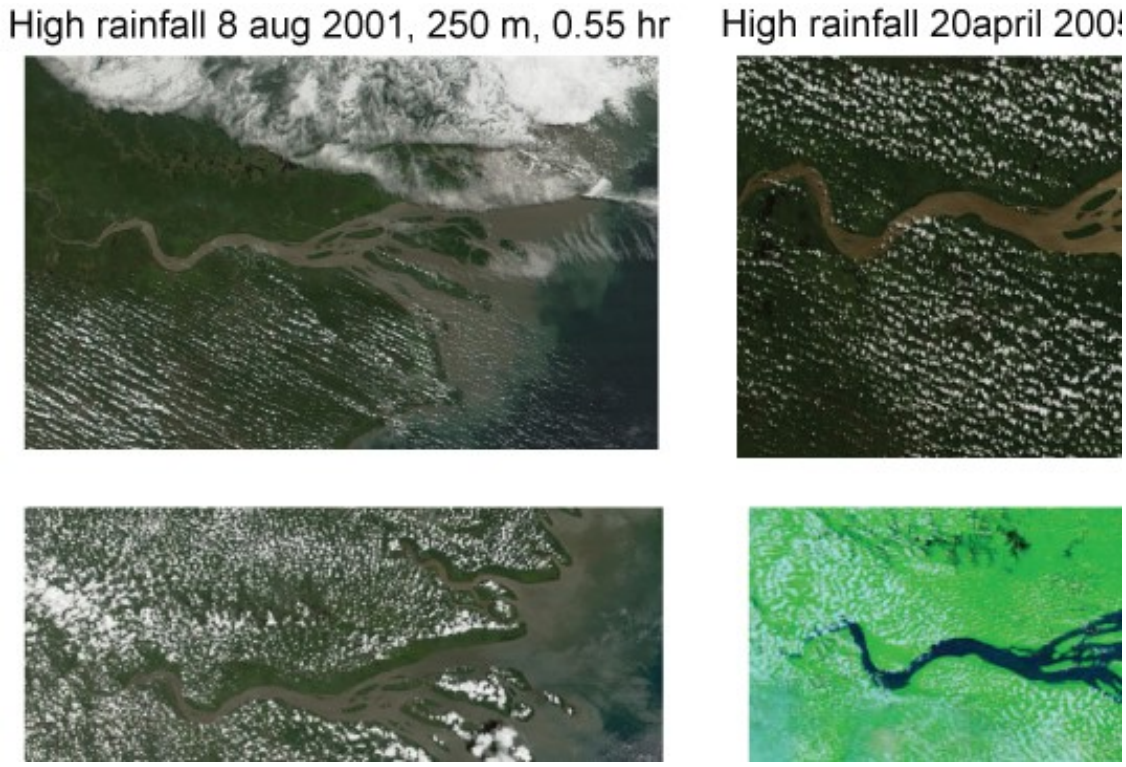


*Figure 3.2 Satellite images from low and high rainfall periods with their resolution and date and time of measurement.*

It can be observed that at both high and low flow the main mangrove islands are still observable. Also, the width of the channels appears relatively constant at either high or low discharge. It was also observed that no significant morphological changes have been occurred in the 5 years time period.
The discharge dynamics of the Fly River are generally not very pronounced. However, during El Niño years the normal cloud cover is greatly reduced and severe droughts developed over Papua New Guinea in 1896, 1902, 1914, 1940-41, 1961, 1972, 1982, 1987, 1997 and 2003. In 1997, which was an El Niño year, a significant drought occurred in the Fly River area, causing a reduction in river flow to approximately 1000 $m^3/s$ *(Dietrich et al., 1999).*

## 3.4 Sediment load

Sediment load data is essential input for modeling the transport and sedimentation pattern in the Fly delta. Sediment load data was measured at Kuambit in the upper part of the Fly River *(Harris et al., 2004).* The suspended sediment concentrations vary as a function of the discharge, the greatest concentrations occurring in June-August. The total river sediment load discharge at the delta apex is estimated by Harris et al., 1993 to be ~85 mln tonnes per year. About 90% of this sediment load is fine-grained (<0.1 mm) suspension load. Harris et al., 2004 calculated the bedload transport rates with a variation of the Bagnold's bedload equation, based on near bed current speed measurements and mean grainsize values. Significant bedload transport occurs, but it is locally variable in direction depending on bed topography and ebb- and flood tidal currents.

Alternatively, Syvitski et al., 2005 use the water balance model mentioned above combined with an empirical relation to relate the catchment area, the basin relief, and the mean basin temperature and total discharge to the river sediment load, yielding seasonal suspended sediment load predictions *(see Fig. 3.3).* They note a tremendous impact of humans on the sediment load of the Fly River. The pre-human sediment load is predicted at only 8 mln tonnes annually, whereas the modern-day sediment load is predicted to be 115 mln tonnes annually, due to mining activities. Harris et al., 1993 corroborate a high sediment load estimate due to mining (125 mln tonnes/year).

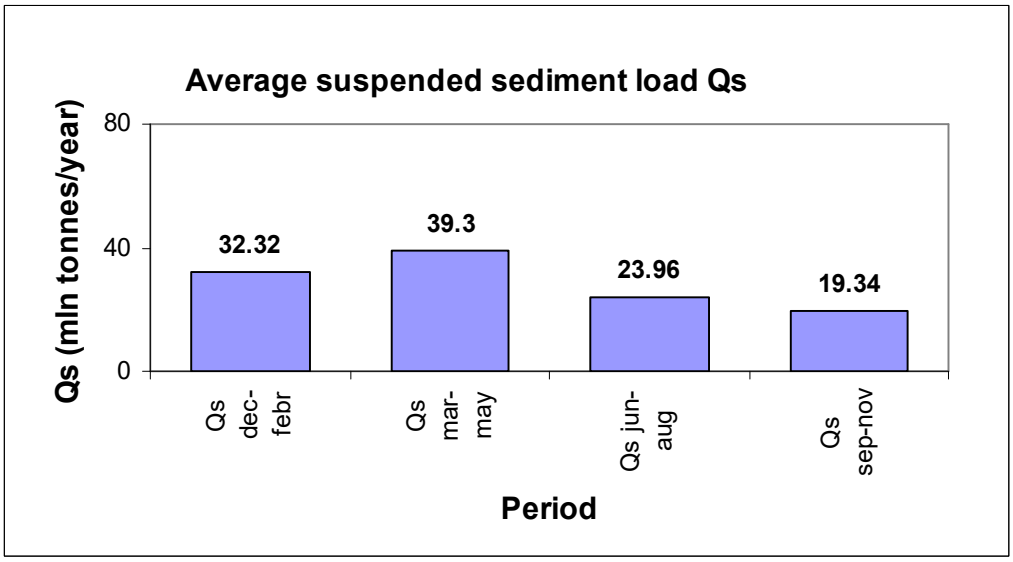


*Figure 3.3 Predicted seasonal suspended sediment load (modified after Syvitski et al., 2005).*

## 3.5 Waves

The influence of waves is minimal; they have only significant impact when surface waves generated by southeasterly trade winds rework the mud and sand on the delta front deposits (from March to November). Most of the fine sediments are brought into suspension due to their influences. During the northwest monsoon (from December to March) minimal surface wave activity results in the deposition of a mud drape (*Harris et al., 1993)*. Although the waves do have some influence, it has been determined that tidal currents have a dominant role in controlling sediment dispersal and deposition (*Harris et al., 1993)*. The significant wave height near the Fly delta area during the southeast trade wind season is 1.3 m, whereas during the south-west monsoon it is only 0.3 m *(Baker et al., 1995)*.

## 3.6 Tidal range and tidal currents

Tidal data consist of tidal range and tidal current data. Tidal range data is published in Harris et al., 1993; Walsh et al., 2004; Wolanski et al., 1995 and Dalrymple et al., 2003 and is used as input data in the Delft3D model experiments. It includes tidal range measurements during spring and neap tide at several locations within the Fly delta area over different measuring campaigns. Peak to trough fluctuation is up to 4 m during spring tides and 1 m at neap tides. The tidal harmonic analysis as described in Wolanski et al., 1997 shows that the M2 and the S2 tide are dominant in the Fly delta area. The M2 and S2 tides are the two main semi-diurnal tides. The M2 tide is the principal lunar tide with a period of 12 solar hours, while the S2 tide is the principal solar tide with also a period of 12 solar hours *(Bearman, 1989).* The M2 tide accounts for 1.049 m, whereas the S2 tide accounts for 0.587 m *(Wolanski et al., 1997).*
The tidal range varies within the funnel of the Fly delta (Walsh et al., 2004; Harris et al., 1993) as shown in *Fig. 3.4*

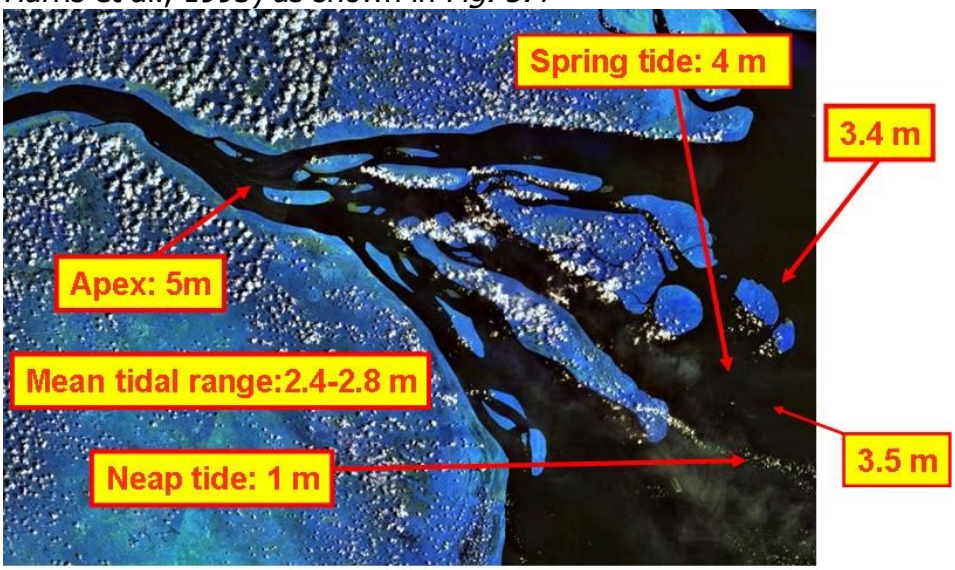


*Figure 3.4 Tidal range data of the Fly delta*

Tidal currents and water velocities are dynamically modeled in our experiments. The model needs to generate realistic stream velocities, which are being validated against the observations. The tidal current data has been collected by studies of Dalrymple et al., 2003; Harris et al., 2004 and Baker et al., 1995, where self-recording current meters where deployed one meter above the bottom at a number of characteristic locations within the Fly delta. These data are given below in *Fig. 3.5.*

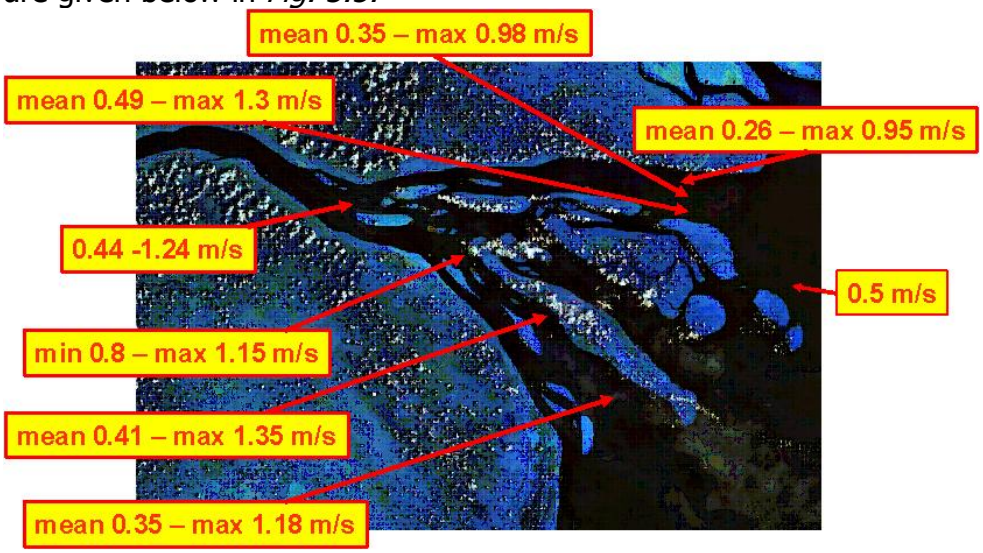


*Figure 3.5 Tidal current measurement data*

## 3.7 Sedimentation rate

Sedimentation rate data is used for validation of the Delft3D simulations. Sedimentation rate data was calculated in Harris et al., 1993, with the $^{210}Pb$ and $C^{14}$ isotopic analyses methods (*Fig. 3.6).* Walsh et al., 2004 distinguish sedimentation rates for the high-, mid-and low tidal zones based on shallow cores and $^{210}Pb$. They measured relatively lower sedimentation rates in the high-tidal zone (1.8 -1.5 cm/year) and low-tidal zones (1.2-1.0 cm/year) as compared to the rates in the mid-tidal zone (3.9-4.4 cm/year).

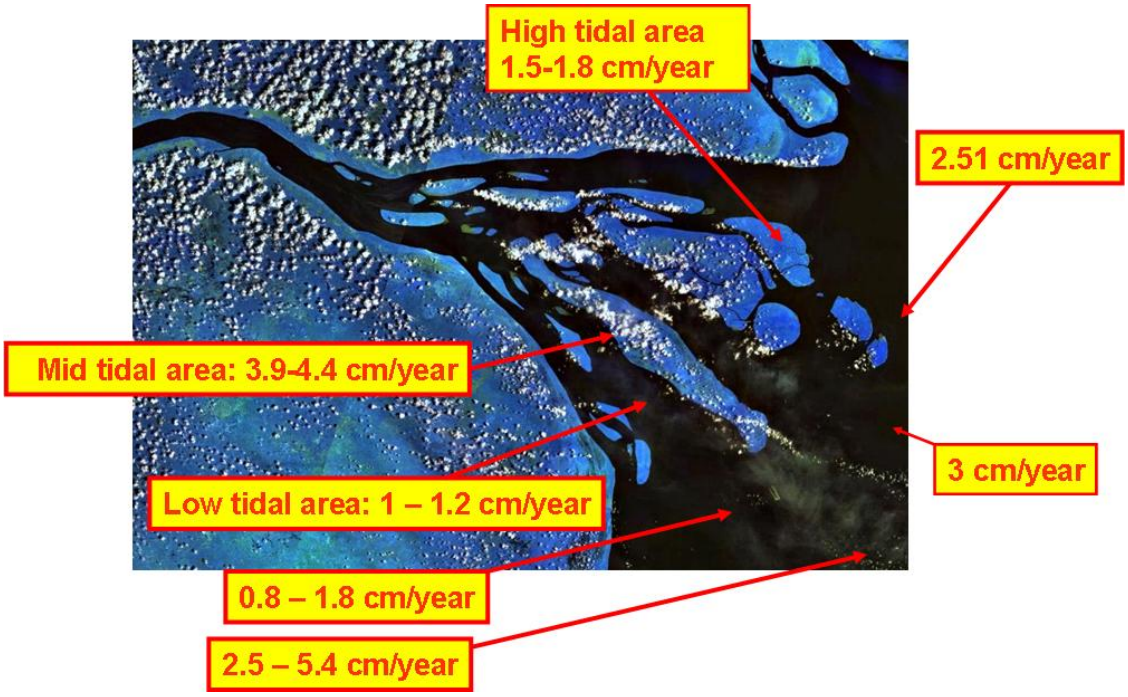


*Figure 3.6 Sedimentation rate data (modified after Walsh et al., 2004 and Harris et al., 1993).*

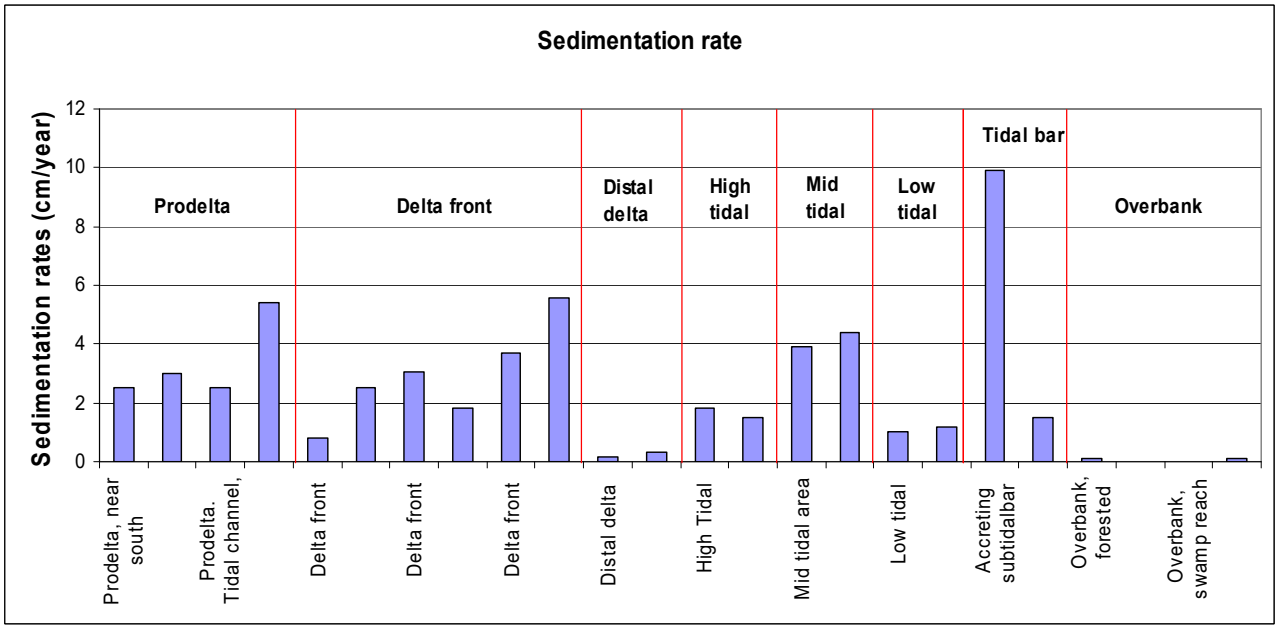


*Figure 3.7 Sedimentation rate data for the Fly delta environment as distinguished for deltaic subenvironments (modified after Harris et al., 2004, Walsh et al., 2004 and Dietrich et al., 1999).*

The sedimentation rates occurring in the different environments are grouped together to distinguish its changes within a depositional environment Harris et al., 1993 *(see Fig. 3.7 and Fig. 3.8)*

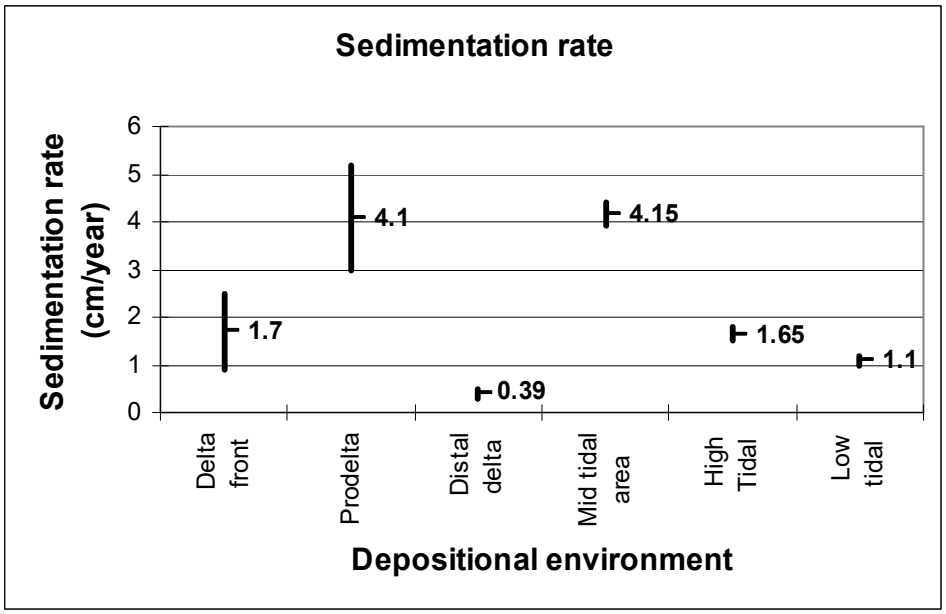


*Figure 3.8 Sedimentation rate data related to their depositional environment (modified after Walsh et al., 2004 and Harris et al., 1993).*

# 4. DELFT3D MODEL CONCEPTS

## 4.1 Introduction

We use the Delft3D package developed at WL|Delft Hydraulics to study sediment transport and storage in the Fly delta area. Delft3D consists of a number of integrated modules to simulate hydrodynamic flow, which can incorporate both tides and waves and the transport of sediment and morphological changes. This chapter describes the relevant concepts of the process based model which are applied to run short-term numerical simulations for this specific study.

## 4.2 Hydrodynamic flow

Delft3D-Flow is the module that performs hydrodynamic computations. The numerical hydrodynamic model solves the unsteady shallow water equations in two dimensions (the so-called depth-averaged approach) or in the full three dimensions. The system of equations consists of the horizontal equation of momentum, the continuity equation and the transport equation for conservative constituents. These equations are expressed in Cartesian rectangular coordinates (x,y).

The vertical $\sigma$- coordinate is scaled as ($-1 \le \sigma \le 0$):

$$\sigma = \frac{z - \zeta}{h}, \text{ (Lesser et al, 2004)} \qquad (4.1)$$

where

$\sigma$ = Vertical "sigma" coordinate

$\zeta$ = Water surface elevation above reference datum (m)

z = Vertical Cartesian coordinate (m)

h = water depth (m)

The vertical momentum equation is reduced to the hydrostatic pressure relation, it is assumed that vertical accelerations are small compared to the gravitational acceleration and are not taken into account. The resulting formula is then equal to (Lesser et al., 2004):

$$\frac{\partial P}{\partial \sigma} = -\rho g h \qquad (4.2)$$

P = Pressure (Pa)

$\sigma$ = Vertical "sigma" coordinate

$\rho$ = Local fluid density (including salinity, temperature and sediment) (kg/m$^3$)

g = acceleration of gravity (m/s$^2$)

The horizontal momentum equations are as follow *(Lesser et al., 2004):*

$$\frac{\partial U}{\partial t}+U\frac{\partial U}{\partial x}+v\frac{\partial U}{\partial y}+\frac{\omega}{h}\frac{\partial U}{\partial \sigma}-fV=-\frac{1}{\rho_o}P_x+F_x+M_x+\frac{1}{h^2}\frac{\partial}{\partial\sigma}(\nu_v\frac{\partial u}{\partial\sigma}) \quad (4.3)$$
$$\frac{\partial V}{\partial t}+U\frac{\partial V}{\partial x}+V\frac{\partial V}{\partial y}+\frac{\omega}{h}\frac{\partial V}{\partial \sigma}-fU=-\frac{1}{\rho_o}P_y+F_y+M_y+\frac{1}{h^2}\frac{\partial}{\partial\sigma}(\nu_v\frac{\partial v}{\partial\sigma})$$

U,V = generalized Lagrangian mean horizontal velocity components (m/s)
f = Coriolis coefficient (inertial frequency) ($s^{-1}$)
$\rho_o$ = Reference density of water ($kg/m^3$)
u, v = Eulerian horizontal velocity components in Cartesian coordinates (m/s)
$\nu_v$ = Kinematic viscosity ($m^2/s$)
$\omega$ = Vertical velocity component in sigma coordinate system ($s^{-1}$)
x, y = Cartesian rectangular coordinates
t = time (s)

The formulas for the horizontal pressure terms $P_x$, $P_y$ and the horizontal Reynold's stresses $F_x$, $F_y$ are further explained in Lesser et al., 2004.

The depth-average continuity equation is given by Lesser et al., 2004:

$$\frac{\partial\zeta}{\partial t}+\frac{\partial\left[h\bar{U}\right]}{\partial x}+\frac{\partial\left[h\bar{V}\right]}{\partial y}=S \quad (4.4)$$

Here S represents the contribution per unit area due to discharge of water.
$\zeta$ = Water surface elevation above reference datum (m)
$\bar{U},\bar{V}$ = depth-average Lagrangian mean velocity components (m/s)

The advection-diffusion transport equation is equal to:

$$\frac{\partial[hc]}{\partial t}+\frac{\partial[hUc]}{\partial x}+\frac{\partial[hVc]}{\partial y}+\frac{\partial[\omega c]}{\partial\sigma}=$$
$$h\left[\frac{\partial}{\partial x}\left(D_H\frac{\partial c}{\partial x}\right)+\frac{\partial}{\partial y}\left(D_H\frac{\partial c}{\partial y}\right)\right]+\frac{1}{h}\frac{\partial}{\partial\sigma}\left[D_v\frac{\partial c}{\partial\sigma}\right]+hS \quad \textit{(Lesser et al., 2004)} \quad (4.5)$$

S represents here source and sink terms per unit area.
c = mass sediment concentration ($kg/m^3$)
$\omega$ = Vertical velocity component in sigma coordinate system ($s^{-1}$)
$D_v$, $D_h$ = Horizontal and vertical diffusion coefficient ($m^2/s$)

## 4.3 Sediment transport

The sediment transport q (kg/m$^2$s$^2$) consist of bedload sediment transport (sand) $q_{b,c}$ and suspended load transport (fine-grained sediment) $q_{s,c}$.

A modified expression for the bed load transport rate is given here as follow:

$q_{b,c} = 0.1\,(s-1)^{0.5}\, g^{0.5}\, d_{50}^{1.5}\, D_*^{-0.3}\, T^{1.5}$ for $T \geq 3$ (van Rijn, 1993) (4.6)

in which:

| | |
|---|---|
| $q_{b,c}$ | = volumetric bed load transport rate (m$^2$/s) |
| $T = (\tau'_{b,c} - \tau_{b,cr})/\tau_{b,cr}$ | = dimensionless bed-shear parameter |
| $\tau'_{b,c} = \rho g\left(\bar{u}/C'\right)^2$ | = effective bed-shear stress (N/m$^2$) |
| $C'$ = 18 log (12 h/3$d_{90}$) | = grain related Chézy-coefficient (m$^{1/2}$/s) |
| $d_{50}$, $d_{90}$ | = particle diameters (m) |
| $\bar{u}$ | = depth-averaged velocity (m/s) |
| $\tau_{b,cr}$ | = critical bed-shear stress (N/m$^2$) |
| $D_* = d_{50}\left[(s-1)g/\nu^2\right]^{1/3}$ | = dimensionless particle parameter (-) |
| $s = \rho_s/\rho$ | = relative density (-) |
| $\rho_s$ | = sediment density (kg/m$^3$) |
| $\nu$ | = kinematic viscosity coefficient (m$^2$/s) |

Due to the absence of waves the direction of the bedload transport is taken to be parallel with the flow in the bottom layer and so in the direction of maximum flow velocities. The bed load transport is consisting of the bottom layer bedload components:

$$q_{b,m} = \frac{u_{b,m}}{|u_b|}|q_b| \quad \text{and} \quad q_{b,n} = \frac{u_{b,n}}{|u_b|}|q_b| \tag{4.7}$$

where $u_{b,n}$ , $u_{b,m}$ and $|u_b|$ are the local bottom layer flow velocity components

Sedimentation occurs when the bed shear stress is smaller then the critical stress and erosion occurs when bed shear stress is larger then the critical stress.

The depth-averaged suspended load transport ( $q_{s,c}$ ) is defined as the integration of the product of velocity (u) and concentration (c) from the edge of the bed load layer (z=a) to the water surface (z=h) as follow:

$$q_{s,c} = \int_a^h uc\,dz, \text{ (van Rijn, 1993)} \tag{4.8}$$

in which:

$q_{s,c}$ = volumetric suspended load transport ($m^2/s$)
u = fluid velocity at height z above bed
c = sediment concentration (volume) at height z above bed

The concentration can be given as weight concentration ($c_g$) in $kg/m^3$ or as a volume concentration ($c_v$) in $m^3/m^3$. These two are related as $c_g = \rho_s c_v$ (4.9)

## 4.4 Tide generation

Tidal range of neap-spring tidal cycle varies as function of time, which is mainly caused by astronomical effects. This neap-spring tidal cycle is important for the sediment transport calculations in tidal conditions. A power-law relation is assumed between sediment transport ($q_t$) and depth average velocity ($\bar{u}$) and is given in the following formula:

$q_t = a\bar{u}^b$ (van Rijn, 1993) (4.10)

Calculation of depth averaged flow velocity ($\bar{u}$) during each daily tidal cycle is based on the formula: $\bar{u}=\hat{u}\sin(\omega t)$ (van Rijn,1993) (4.11)
in which:
$\bar{u}$ = current velocity at the time t of a daily tidal cycle (flood/ebb)
$\hat{u}$ = maximum current velocity of a daily tidal cycle (flood/ebb)
$\omega = 2\pi / T_m$ = angular frequency
$T_m$ = duration of a tidal cycle

The astronomical tide calculation is done with the following formula:

$$H(t) = A_o + \sum_{i=1}^{k} A_i.F_i.\cos(\omega_i.t + (V_o + u)_i - G_i)$$ (Delft3D Flow manual, 2005) (4.12)

H(t) = water level at time t
$A_o$ = mean water level over a certain period
k = number of relevant tide types
i = index of a tide
$A_i$ = local tidal amplitude of a tide
$F_i$ = nodal amplitude factor
$\omega_i$ = angular velocity
$(V_o + u)_i$ = astronomical argument
$G_i$ = improved kappa number
For the simulations only the amplitudes, phases and frequencies are necessary in terms of tide names.

## 4.5 Numerical solution

The mathematical flow and sediment transport equations as described earlier are solved in Delft3D-Flow numerical model. First the equations are discretized in space by covering the model area with a rectangular grid. It is assumed that the grid is orthogonal. During discretizing the variables are arranged in a pattern called the Arakawa-C-grid (a staggered grid). Here, the water level points are defined in the centre of a cell; the velocity points are perpendicular to the grid cell faces where they are situated *(see Fig. 4.1).*

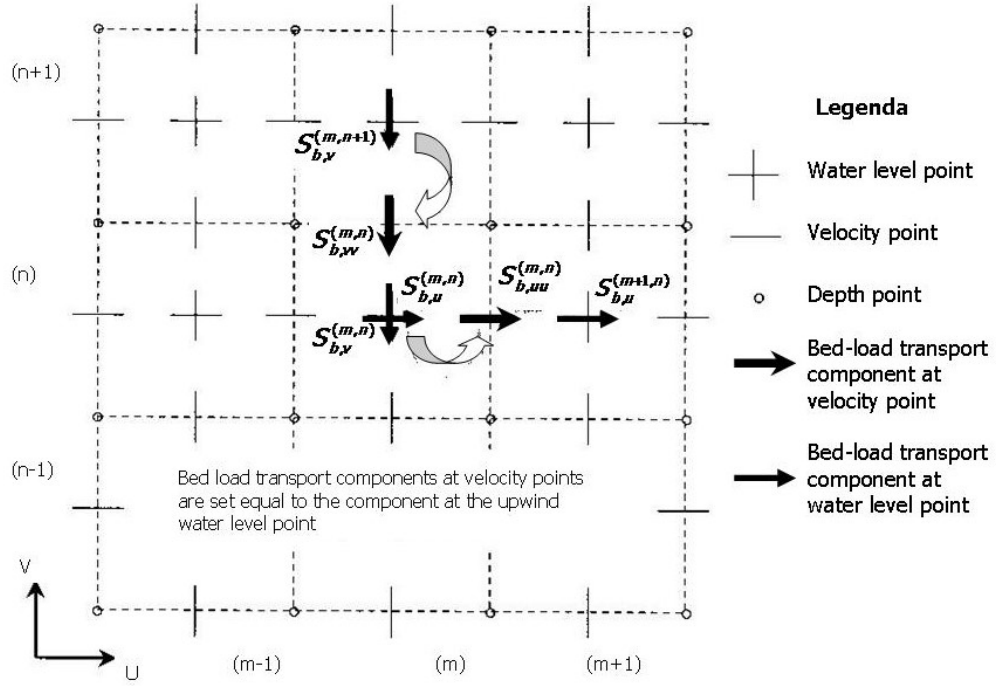


*Figure 4.1 Conceptual Delft3D staggered grid with bedload sediment transport components at velocity points (modified after Lesser et al., 2004)*

The continuity and horizontal momentum equations are solved with an alternating direction implicit (ADI) method. This method couples the implicitly integrated water levels and velocities along the gridlines. An extension of this method with a special approach for the horizontal advection terms, called the cyclic method, was used during the simulations.

# 5. Delft3D MODEL EXPERIMENTAL SET UP

## 5.1 Gridding and Bathymetry Input

Gridding has been done in Delft3D-RGFGRID module. A rectangular grid in Cartesian coordinates has been created. The number of grid cells in M (X)-and N (Y) direction and the length of each grid cell were assigned as in Table 2.
The grid is scaled to a size of approximately 20 ×20 km, which is only ~10 % compared to the actual Fly delta dimensions. This scaling has been done because the intention was to use a simple hypothetical model that allows fast computations. The model grid is supposed to be representative for a number of tributaries in a deltaic system like the Fly delta.

| **Grid parameters** | | **Bathymetric parameters** | |
|---|---|---|---|
| M-direction | 70 | Channel depth (in m) | -10 |
| N-direction | 114 | Channel Width (in m) | 1000 |
| Length of grid cells (in m) | 200 | Island Height above sea level (in m) | +2 |
| Total amount of grid cells | 6923 | Offshore Depth (in m) | -50 |

*Table 2 Model grid parameters*

To avoid numerical instability during the simulations, the grid is refined and smoothed especially in the channel areas. Two types of grids were generated; one with a straight channel delta geometry and another one with funnel-shaped delta geometry. For the funnel shape channel geometry two types of bathymetric values were assigned; a funnel with islands and one without islands.
Subsequently, depths values were assigned for the channel and funnel shape area. It is obvious that the downscaling of the channel geometry needs to maintain hydrodynamically accurate conditions. Hence, the modeled discharge and the associated channel geometry are scaled as to represent water velocities ranging between 0.5 – 1.5 m/s.
The land area on both sides of the channels was manually defined as drypoint area, +2 m above sea level, because in this study the focus is on the sedimentation and erosion pattern in the delta distributaries. For the nearshore prodelta part of the grid linear interpolation was applied to define the bathymetry from -10 m to -50 m. The generated grids with their dimensions and bathymetric values are shown below in *Fig. 5.1.*

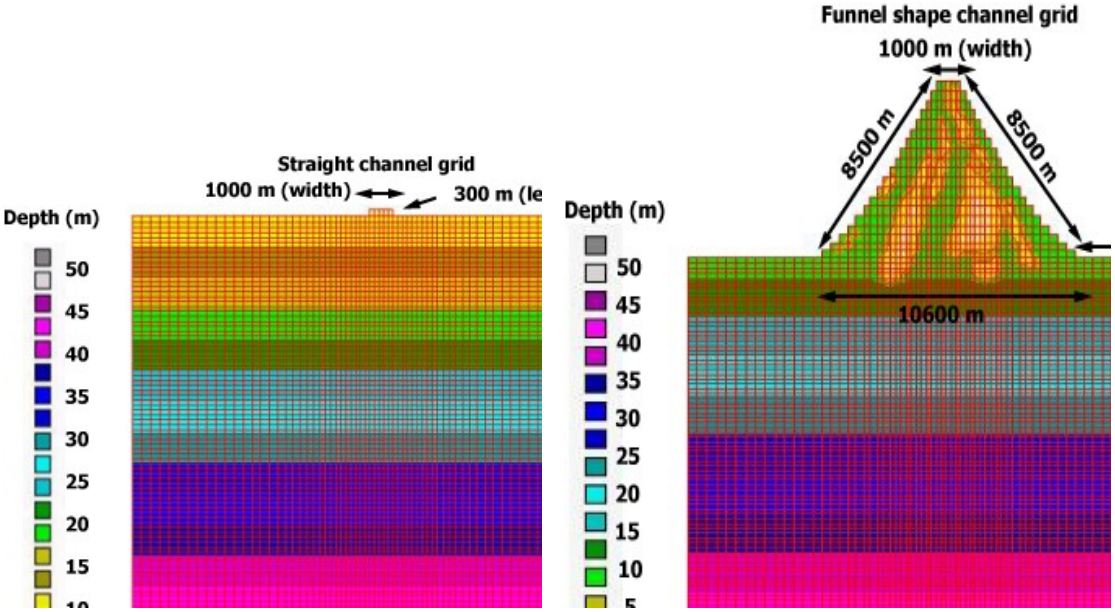


*Figure 5.1 The straight channel delta and funnel-shaped delta grids with bathymetric values*

## 5.2 Fixed Input Parameters

The data input required for running simulations in Delft3D needs to be stored in an input file called the Master Definition File (MDF). The required parameters are obtained from the literature data as described in the previous chapter. Many additional parameters and constants remain as default values or have been established by running a number of sensitivity tests. Here we list the parameters that are fixed for all experiments and scenarios.

The fixed input parameters are related to 1) the simulation run time, 2) the sediment types, 3) physical parameters related to the sediment transport.
The simulation time of all experiments is defined to be 3 months. Delft 3D uses an upscaling approach that scales the speed of the changes in the morphology up to a rate that it begins to have a significant impact on the hydrodynamic flows *(Roelvink, 2006).* This upscaling factor is called the morphological scale factor. At each time step the erosion and deposition fluxes are multiplied by the scale factor allowing accelerated bed level changes to be incorporated dynamically in to the hydrodynamic flow calculations. This makes it possible to execute simulations for longer time intervals with the aim to bridge the time difference between short-term hydrodynamic and transport processes, varying over hours and days, and morphological changes which occur over much longer time intervals. The morphological factor allows us to generate simulation results on a somewhat longer timescale. In our experiments a morphological scale factor of 4 has been used, implying that our 3 month experiments represent a time period of 1 year. Figure 5.2 shows the effect of applying a greatly increased

morphological scale factor (i.e. 4 resulting in 1 year of sediment deposition versus 40 resulting in 10 years of sediment deposition).
Deposition increases linearly and channel evolution is evident over the longer time period.

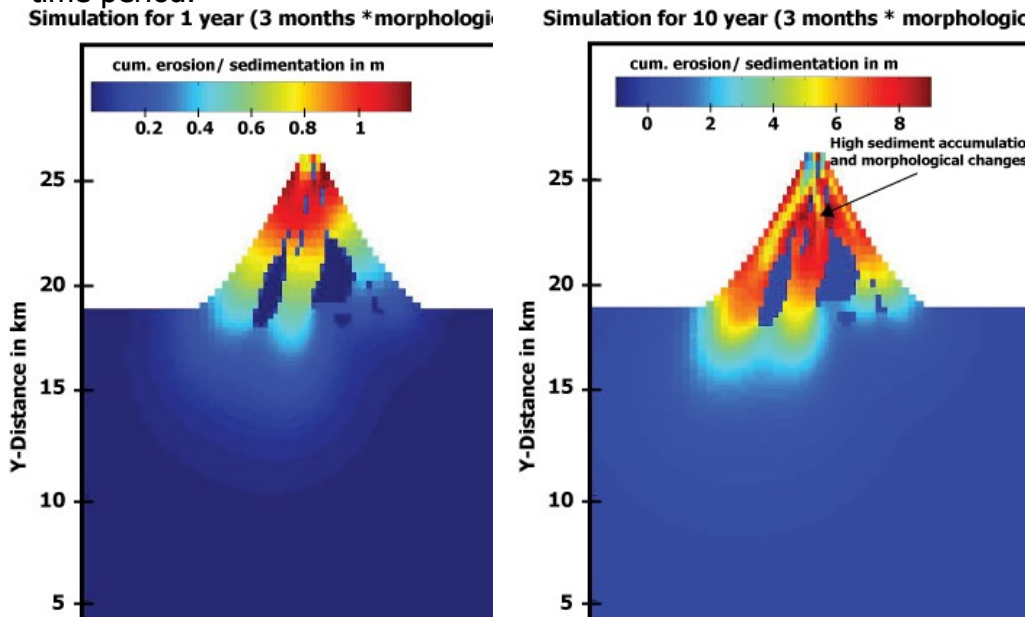


*Figure 5.2 Influences of morphological factor value*

Two sediment types were defined: non-cohesive sediment sand and cohesive sediment clay. The reference density and specific density for clay and sand both are set at respectively 1600 and 2650 kg/m$^3$. Sand is estimated to have a median grainsize of 200 $\mu$m.
Specifically for non-cohesive sediment the erosion rate ($1 \times 10^{-5}$ kg/m$^2$/s) and settling velocity (at 0.15 mm/s) are specified. In addition, the critical bed shear stress for sedimentation (1 N/m$^2$) and erosion (0.5 N/m$^2$) are set after running a number of sensitivity tests.
A number of physical parameters remain at default values, i.e. the gravitational constant at 9.81 m/s$^2$, river water density at 1000 kg/m$^3$. The Chezy equation has been used for modeling the resistance of the flow.
Lastly, some initial conditions need to be defined: initial sediment concentrations set to zero, with a 12 hour spin-up period to establish a equilibrium in the velocity and concentration field. Also, an initial depth for the sediment layer that can be eroded has to be defined, consisting of cohesive sediment and non-cohesive sediment. Both are set at 5 m depth.

## 5.3 Simulation scenarios

### 5.3.1 Introduction

To study the effects of different controlling factors like river discharge and sediment load, tide ranges and morphology a number of scenarios were simulated.
The scenarios are evaluated to find conditions that are a representative model for the Fly delta area. Especially for selecting the base case scenario the parameters settings are adjusted until the modeled values of flow velocity and sedimentation rate became in range with measured values.
Then a base case scenario has been chosen, which is used to investigate 1) the influence of different initial morphology 2) the influence of high and low river discharge and sediment load, 3) the influence of the tidal conditions by running the base case scenario for no tide, one tide and two tides.
The scenarios are compared by evaluating the difference in the total amount of sediment deposited in the model grid for the 1 year experiments. We compare the amount of sediment deposited in the model grid for the 1 year experiment of the base case with the grids for the scenarios by subtracting, this is the so-called 'difference grid'. Another way of comparing the different scenarios is to study specific grid cells, i.e. 'observation stations', where bedlevel and water level changes are being recorded every 360 minutes during the experiment. The observation stations are strategically located in specific parts of the delta such as in the distributary channels, near the tidal islands, in the distal as well as proximal part of the delta.

### 5.3.2 Sediment load scenarios

Four scenarios were simulated to select appropriate conditions for discharge and sediment load. One of these scenarios was subsequently use as a base case scenario.
The estimates for water discharge of the Fly River vary between 4500 $m^3/s$ *(Syvitski ey al., 2005)* to 7000 $m^3/s$ *(Harris et al., 1993, Harris et al., 2004).* We consider our scaled grid as only a smaller subsystem of the Fly system and transport only 50% of the total water flux.
The estimates for the total annual sediment load of the Fly River vary an order of magnitude: a predicted 115 mln tonnes/year for the 'modern' load, strongly influenced by mining activities *(Syvitski et al., 2005)*, 85 mln tonnes/year based on extrapolation of sediment load measurements at a station 300 km upstream the river *(Harris et al., 1993)* to a prediction of a 'pre-human' sediment load of only 8 mln tonnes/year *(Syvitski et al., 2005)*. To investigate a reliable range of conditions another scenario with values between the ranges of values was also simulated the "intermediate load" scenario.

The sediment concentration (kg/m$^3$) for these scenarios is calculated as follows:
Qs/ (Q* t), (4.13)
where Qs = sediment load (kg/year)
Q = river discharge (m$^3$/s)
t = time in seconds (60 sec*60 min*24 hours*365 days)
The total sediment load is divided in a bedload and suspended load component; 20 % was considered as bedload material (sand) and 80 % as cohesive suspended load material (clay). The water discharge and sediment concentration for sand and clay respectively are given below in Table 3.

.

| **Scenario** | **Sediment load (kg/m$^3$)** | | **River discharge(m$^3$/s)** | **Remarks** |
|---|---|---|---|---|
| | **Sand** | **Clay** | | |
| A | 0.01148 | 0.04592 | 2250 | "Pre-human" (Syvitski, 2005) |
| B | 0.0362 | 0.1448 | 3500 | "Intermediate load" |
| C | 0.077 | 0.308 | 3500 | Harris, 1993 |
| D | 0.1620 | 0.6482 | 2250 | "modern" (Syvitski, 2005) |

*Table 3 Water discharge and sediment load scenarios*

### 5.3.3 Initial delta channel morphology scenarios

The influence of the morphology of the delta distributaries was investigated by running the base case scenario for three different morphologies; a delta funnel shape with a number of islands of +2m elevation, a delta funnel shape without islands and a straight river channel discharging into the marine basin directly *(see Fig 5.1).*

### 5.3.4 Tide scenarios

The selected base case scenario was further used to study the influences of tidal energy on sedimentation in the distributary channels and the delta area. Simulations with no tide, one tidal component, and two tidal components were compared when studying the tidal influences. The base case scenario includes the main lunar M2 tide influence. Two more scenarios were set up to investigate the tidal influences.
One scenario explores the response of the system when no tides are modeled. The second scenario includes two tidal components. The two tidal components are the principal lunar and solar tides *(Wolanski et al., 1997):*

| Scenario | M2 | | S2 | | Remarks |
|---|---|---|---|---|---|
| | Amplitude (m) | Phase (degrees) | Amplitude (m) | Phase (degrees) | |
| Base-case 'one-tide' | 1.05 | 342 | 0 | 0 | "Intermediate load" |
| Base-case 'no-tide' | 0 | 0 | 0 | 0 | "Intermediate load" |
| Base-case 'two-tides' | 1.05 | 342 | 0.59 | 321 | "Intermediate load" |

*Table 4 Tide scenarios*

### 5.3.5 Discharge peaks and low flow scenarios

The influences of seasonal changes in sediment load and river discharge were studied by simulating two scenarios; one for peak flow conditions (+30% River discharge and +50% Sediment load) and one for low flow conditions (-30% water discharge and -50% sediment load). For these scenarios only the river discharge and sediment load conditions were changed relatively in comparison to the base case scenario. The changes for the peak and low flow scenario are given in *Table 5*.

| Scenario | Sediment load (kg/m$^3$) | | River discharge(m$^3$/s) | Remarks |
|---|---|---|---|---|
| | Sand | Clay | | |
| Base-case | 0.0362 | 0.1448 | 3500 | "Intermediate load" |
| Base case +30%/+50% | 0.0724 | 0.2896 | 4450 | 'Peak flow' |
| Base case -30%/-50% | 0.0181 | 0.0724 | 2450 | 'Low flow' |
| Base case -70%/-0% | 0.0362 | 0.1448 | 1000 | 'El Nino' |

*Table 5 Discharge peak and low flow scenarios*

An additional scenario has been formulated to study the influence of extremely low flow during droughts in El Niño years. The only change made in the base case scenario to set up the 'El Niño scenario' was changing the river discharge from 3500 to 1000 m$^3$/s discharge.

### 5.3.6 Hydrodynamic scaling scenario

It proved hard to jusitfy the scaling of the water discharge to a smaller grid while still acknowledging the hydrodynamic conditions. To further explore the effect of this scaling factor we posed another scenario, where we applied a scaling factor of 75% instead of 50% to the 'prehuman' scenario *(Table 6).*

| **Scenario** | **Sediment load (kg/m$^3$)** | | **River discharge(m$^3$/s)** | **Remarks** |
|---|---|---|---|---|
| | **Sand** | **Clay** | | |
| A | 0.01148 | 0.04592 | 2250 | "Pre-human" (Syvitski, 2005) |
| E | 0.01148 | 0.04592 | 3375 | "75% discharge" |

*Table 6 Hydrodynamic scaling scenario, river and sediment load conditions*

### 5.3.7 Medium time scale scenarios

To focus a number of experiments on somewhat longer term morphological changes specifically around a tidal island within the Fly delta we ran two experiments for 10 years. The two experiments that were extended and ran for 10 years are the base case experiment (i.e. experiment B in *Table 3*) and the experiment without any tidal influence (i.e. experiment 'no tides' in *Table 4*).

# 6. RESULTS

## 6.1 Introduction

In this chapter results of the Delft3D model scenarios will be presented. The output consists of time series of specific parameters at specified 'observation points' and of maps of those parameters over the entire simulated grid.
To investigate the simulated results locally in more detail, observation points were placed in the study area. Observations points are specific grid cells where different simulated parameters are recorded and become available for further data analyses. The locations of all observation points are shown in *Fig. 6.1.*

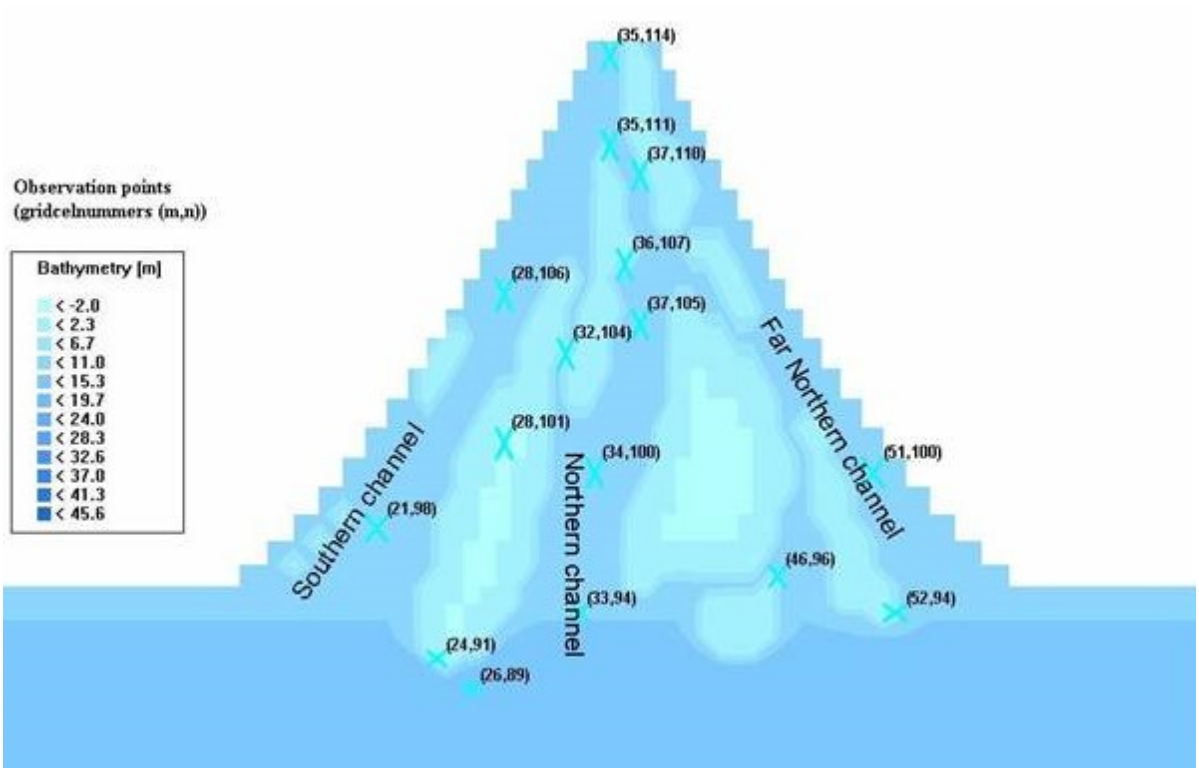


*Figure 6.1 Observation points within the modelled area*

The parameters which are recorded every 360 minutes are the depth-averaged water velocity, the bottom bedlevel, and the waterlevel.
Parameters that were recorded in maps of the entire grid include the cumulative erosion and sedimentation and the available mass of sediment (either specified for the sand component or the clay component).

Based on this output sedimentation patterns can be investigated by creating "difference grids" of the bedlevel change. Difference grids were made in Matlab, where the difference in amount of sedimentation is calculated from the final

bedlevel and initial bedlevel in the delta area *(Fig. 6.2)*. The volume of sediment which has been deposited between these two stages was then calculated in Delft-3D Quickin.

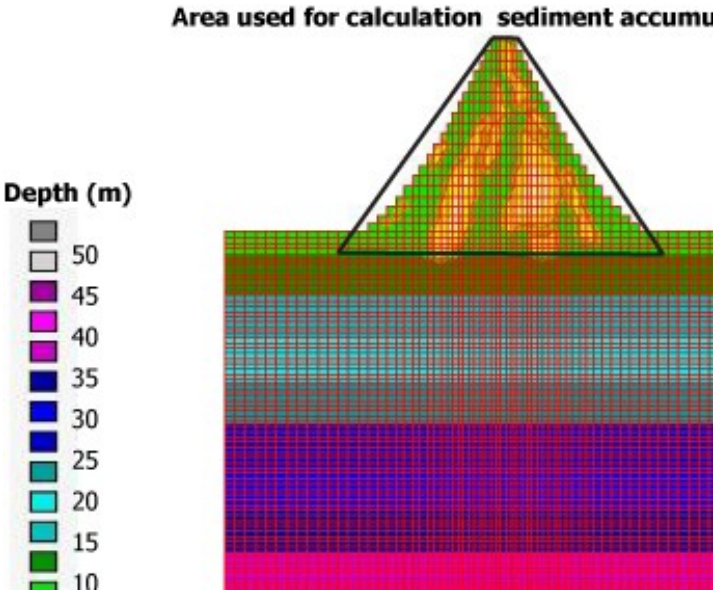


*Figure 6.2 Funnel area considered for sediment accumulation volume*

## 6.2 Sediment load scenarios

### 6.2.1 Total sediment flux scenarios

Four scenarios were simulated to compare the order of magnitude range of sediment flux estimates in the Fly delta that have been posted in previous studies as described in chapter 3.
The aim of these experiments was to compare the depth-averaged velocity and sedimentation rates in the delta distributaries in the model experiment and compare the model predictions with the observed hydrodynamic conditions and reconstructed sedimentation rates. The results of the four scenarios were then also used to determine a base case scenario for the subsequent simulations.

The depth average velocity for a 360 minutes snapshot at the final simulation timestep for the four scenarios is shown below in *Fig. 6.3*. It can be seen that the predicted maximum flow velocity varies between 0.3 -0.6 m/s and occurs near the apex of the delta, where the channels still are relatively narrow. The measured velocities correspond well to mean measured velocities in the apex 0.49 m/s and varying between 0.41-0.26 m/s in the distributaries as presented in *Fig 3.4.* All scenarios show that the rightmost part of the funnel has relatively lower flow velocities. This is generally noted in the field descriptions of the Fly

delta Far Northern channel (mean velocity 0.26 -0.35 m/s) whereas the Southern channel has a slightly higher mean flow velocity (0.41 m/s) (see also Fig 3.4). The scenario that had the lowest discharge and sediment concentration, the so-called Syvitski pre-human' scenario, show the flow velocity to be consistently below 0.3 m/s, which is lower then field observations. The depth-averaged velocities as compared with Fly delta data for the "intermediate load" scenario *(Fig. 6.3B),* Harris scenario *(Fig. 6.3C)* and Syvitski modern scenario *(Fig. 6.3D)* appear feasible.

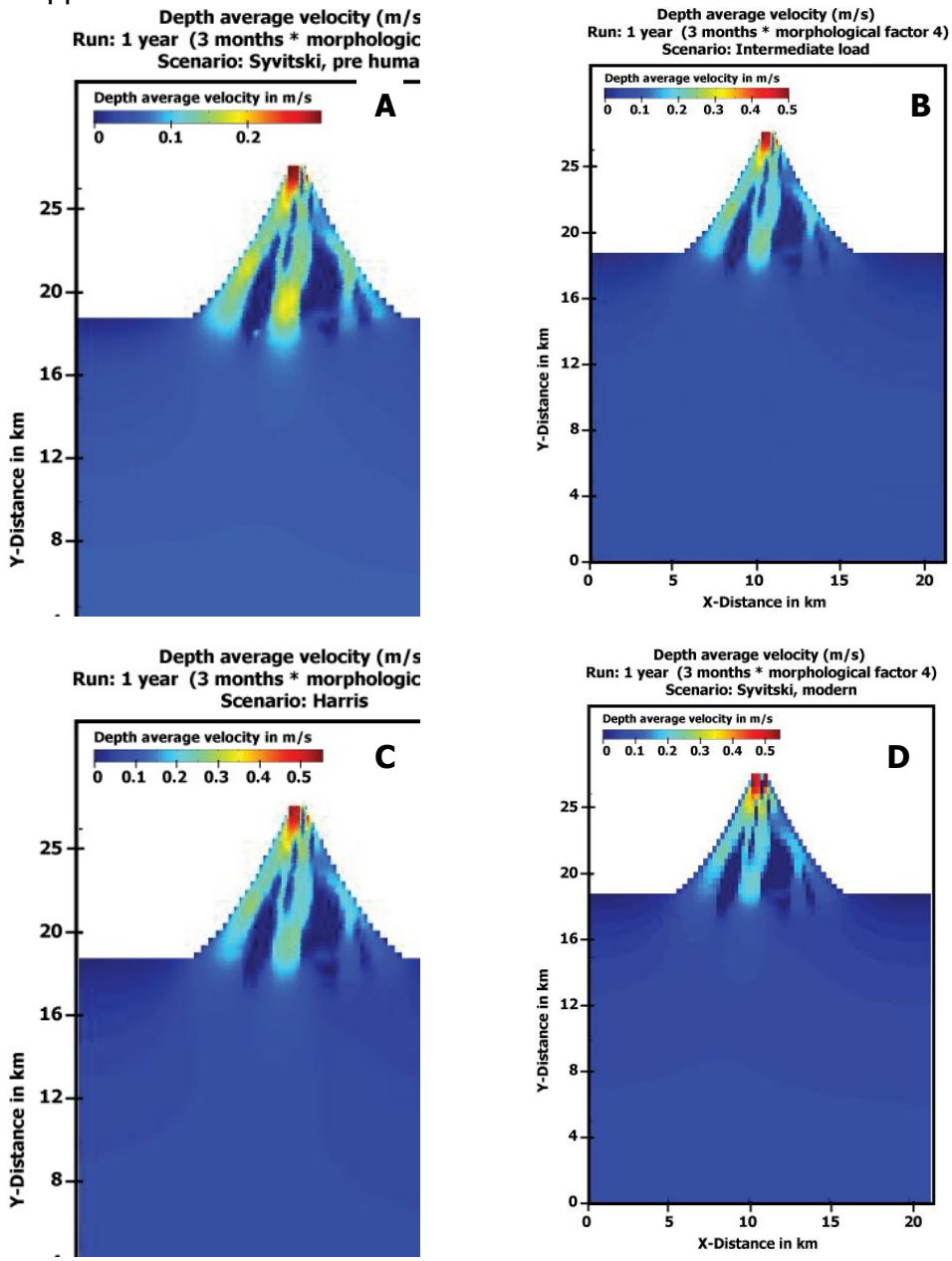


*Figure 6.3 Depth average velocity patterns for four main sediment flux scenarios*

The difference grids of the 4 base case selection scenarios together with the calculated total accumulated sediment volume over the year are given in *Fig 6.4*.
The pattern of sedimentation is rather similar for the four experiments. Higher deposited volumes occur in the delta apex area. Also, the inactive, sheltered nature of the rightmost distributary system is reflected in lower deposited sediment volumes. The sedimentation in the marine basin is relatively low and falls off with distance from the delta front.
The accumulated volume estimates reflect the wide range in input water and sediment flux; scenario A only shows 5 mln $m^3$ accumulated sediment over the year, whereas the most extreme estimate of the sediment flux scenario D shows an accumulation of 57 mln $m^3$.
The sedimentation rate of all scenarios appears higher then field observations. For example, even scenario A that has the overall lowest sedimentation rates shows a significant area in the delta apex that has a sedimentation rate of over 0.3 m/year. The highest sedimentation rate reconstructed by Harris et al., 1993 based on field observations was only 0.1 m/year. Most of the measurements and reconstructed sedimentation rates are even much less and vary from 0.8 – 4.4 cm/year *(Fig 3.7).*

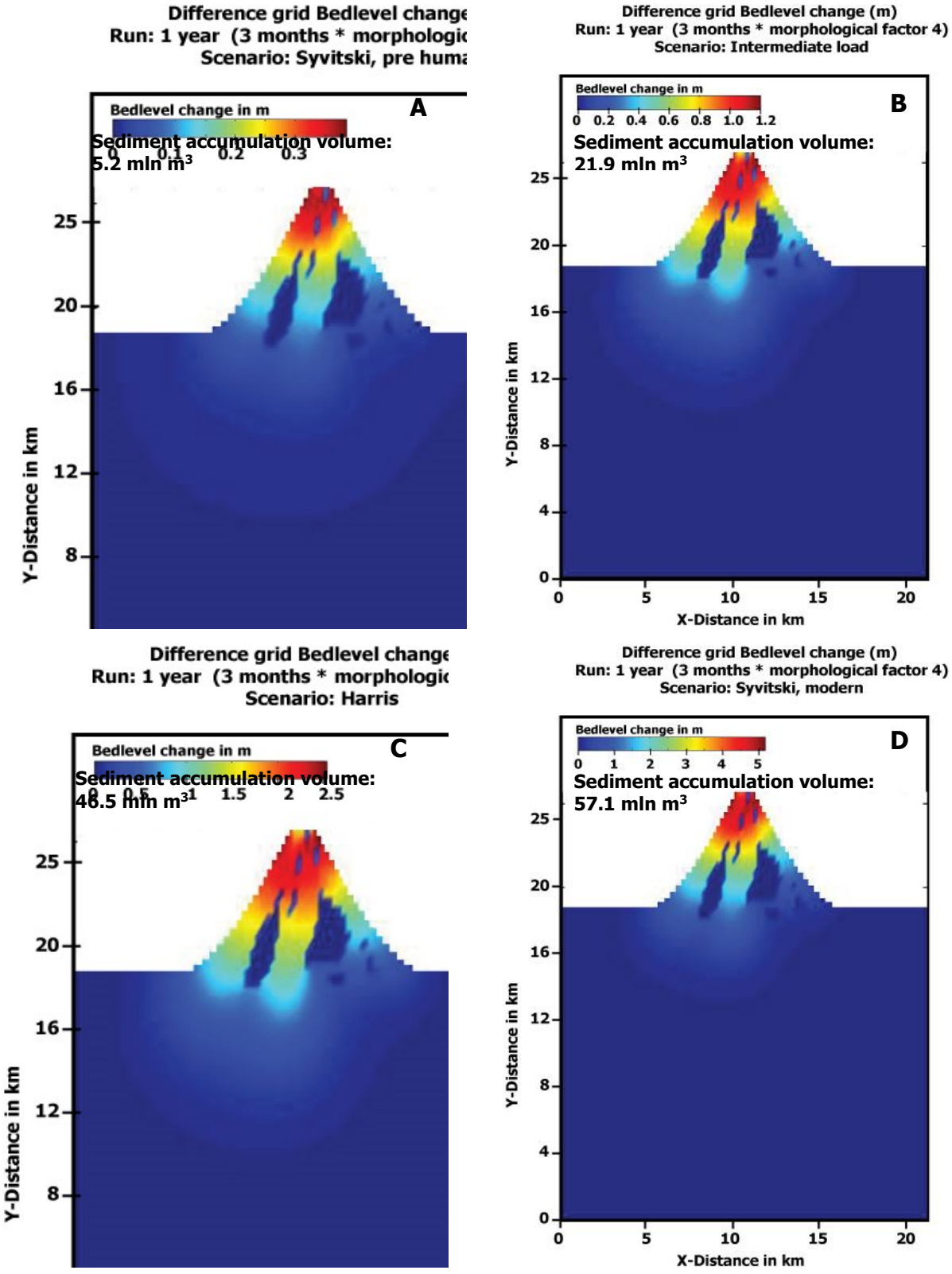


*Figure 6.4 Difference grids and sediment accumulation volume for base case selection scenarios*

After evaluating the sedimentation results and the related depth average velocity trends, it was decided to continue with the "intermediate load" scenario due to the fact that its results match the actual measurements of flow velocity and sedimentation rates of the Fly delta better then results from the other scenarios.

### 6.2.2 Sedimentation pattern for "Intermediate load" scenario

This part is focused on investigating the sedimentation pattern within the funnel delta area for the base-case "intermediate load" scenario. The selected observation points have been chosen in all the distributary channels on three different locations within the funnel shape. These were located in the delta apex, mid-delta area and. channel mouthbar area. The studied observation points are shown in *Fig. 6.5*
All observation points show a bedlevel decrease, which means that sedimentation has occurred and the channel shallowed. The bedlevel changes at all the selected observation points are plotted below in *Fig. 6.6*.

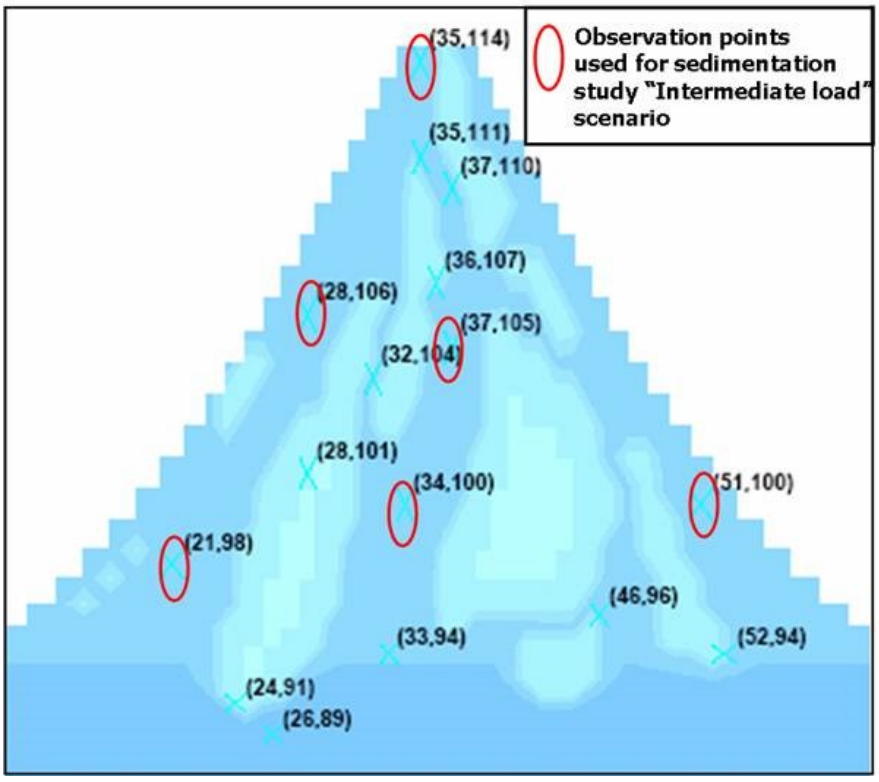


*Figure 6.5 Observation points for studying sedimentation pattern "Intermediate load" scenario*

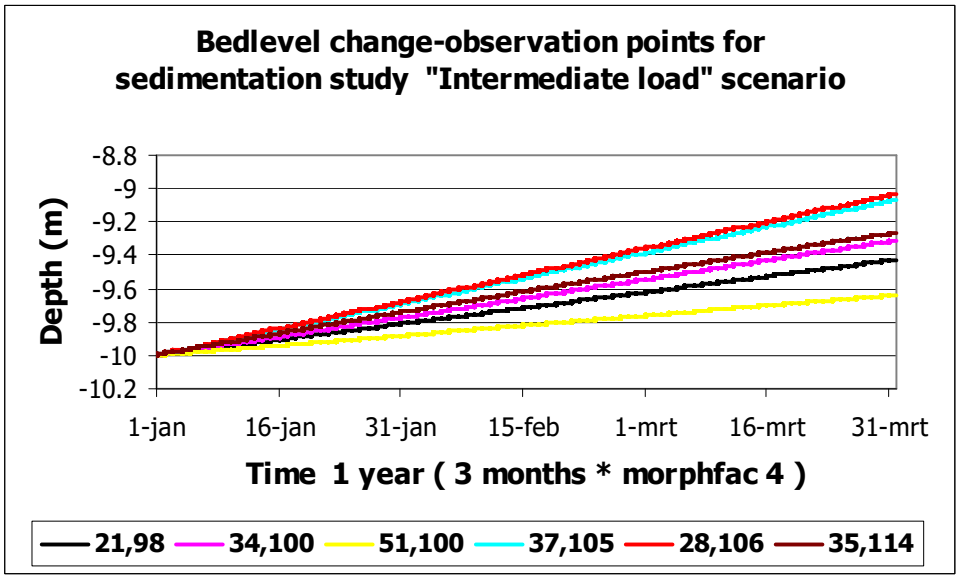


*Figure 6.6 Bedlevel change at observation points for "Intermediate load" scenario*

The sedimentation for the three channels in the channel mouth area is different from each other. It was observed that the largest sedimentation rate occurred for observation point (34, 100) located in the middle channel, which is comparable to the Northern channel in the Fly delta. The smallest sedimentation rate was noticed for the observation point (51, 100) in the rightmost channel, i.e. comparable to the Far Northern channel *(see Fig. 6.6).*
At the mid-delta area, the sedimentation rate for observation point 28, 106 (i.e comparable to the Fly delta Southern channel) is somewhat higher than observation point 37,105 (Northern channel) *(see Fig. 6.6).* However, the sedimentation rates in these observation points are rather similar.
At the delta apex, the sedimentation at observation point 35,114 is lower than that of the mid-delta area, but higher than in the channel mouth area.

When considering each channel separately, the sedimentation for the Southern channel was high in the mid-delta and low in the delta front or channel mouth area. For the middle (Northern) channel the same trend was observed. In contrast, for the rightmost channel, i.e the Far Northern channel in the Fly delta the smallest bed level decrease was observed in the delta front, channel mouth area.
The differences in sedimentation between the three channels are further investigated by comparing the depth-averaged velocity of the three observation points at the channel mouths for a certain time interval. This is shown below in *Fig. 6.7.*

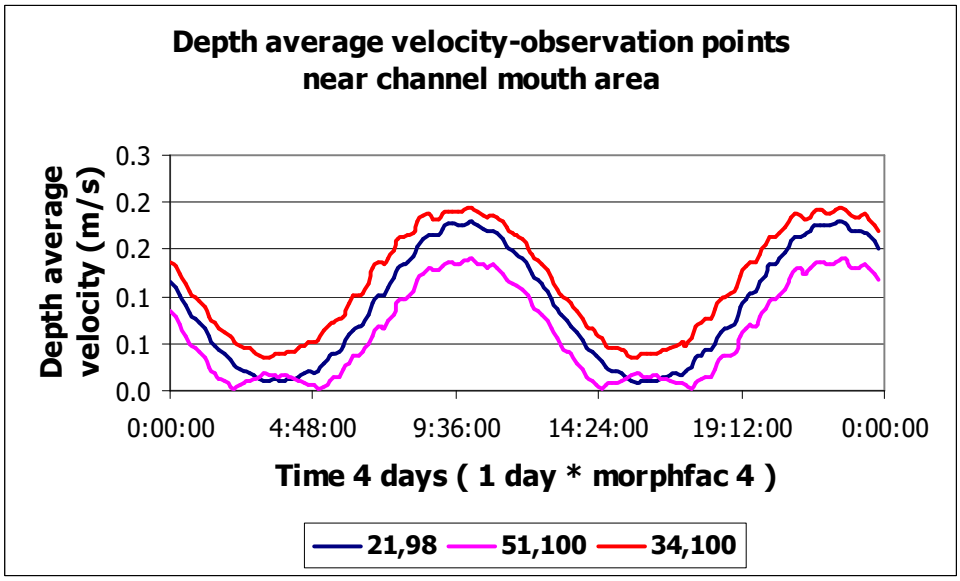


*Figure 6.7 Depth-averaged velocity for three observation points near the channel mouth*

All flow velocities are remarkably low. The lowest depth-averaged velocity is shown for observation point 51,100, near the mouth of Far Northern channel *(see Fig. 6.7).* Despite the low flow velocity, the lowest sedimentation is observed in this observation point. Similarly, the highest depth-averaged velocity is observed for observation point 34,100, near the Northern channel mouth, where the sedimentation was also highest. This implies that the sediment transport is limited due to the generally low velocities and small increases in flow velocity cause a increase in sediment pick-up and subsequent rapid deposition or even an increase in sediment introduced by tidal flux.

The effect of the tidal water flux on the depth-averaged velocity is investigated for point 21,98 at the channel mouth area. The relation between depth-averaged velocity and waterlevel shows that the depth averaged velocity is highest during the slack tide period after the flood tide and lowest during the slack tide period after the ebb tide *(see Fig. 6.8).* This indicates that sediment transport is high during the slack tide after ebb tide and low at the slack tide after flood tide. It is much more diffeicult to have an idea of the sediment that is introduced into the system based on these tidal fluxes; even just after flood tide the depth averaged velocity is still very low.

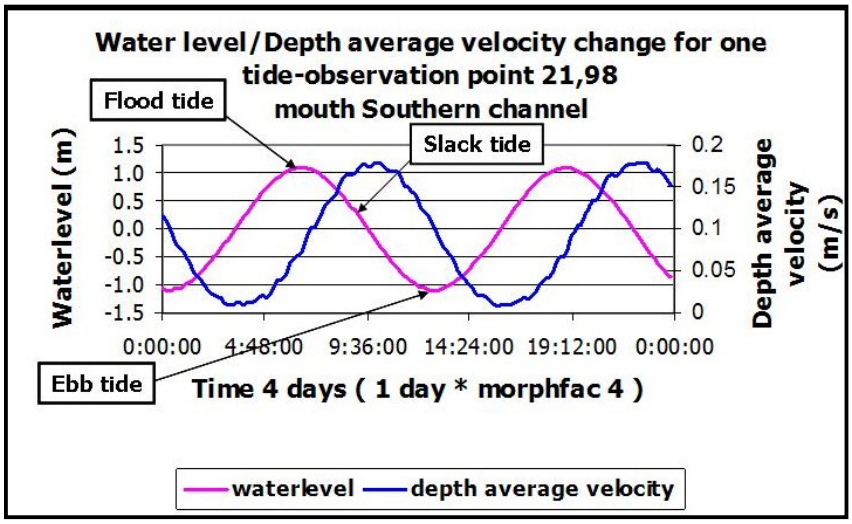


*Figure 6.8 Waterlevel and depth-averaged velocity relation*

## 6.3 Initial delta channel morphology scenarios

The influences of the morphology of the initial delta bathymetry on sedimentation pattern development for base case "intermediate load" scenario, was studied for the grid with the funnel shape with islands, the funnel shape without islands and the straight channel. Three common observation points were selected for studying the bedlevel change *Fig. 6.9.*

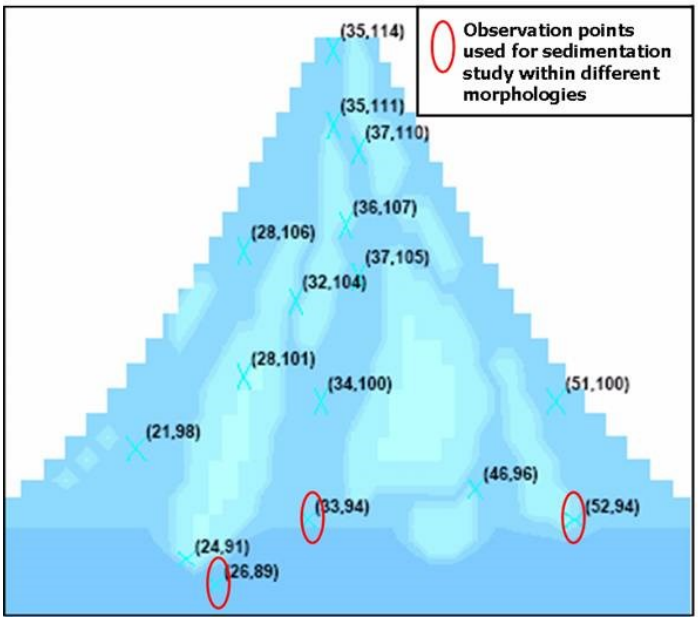


*Figure 6.9 Observation points studied for the different morphological grids.*

The bedlevel changes, the cumulative erosion/sedimentation as well as the depth-averaged velocity have been studied for the three morphologies. The cumulative erosion/sedimentation maps after one year of simulation for the three morphologies are shown below in *Fig. 6.10*

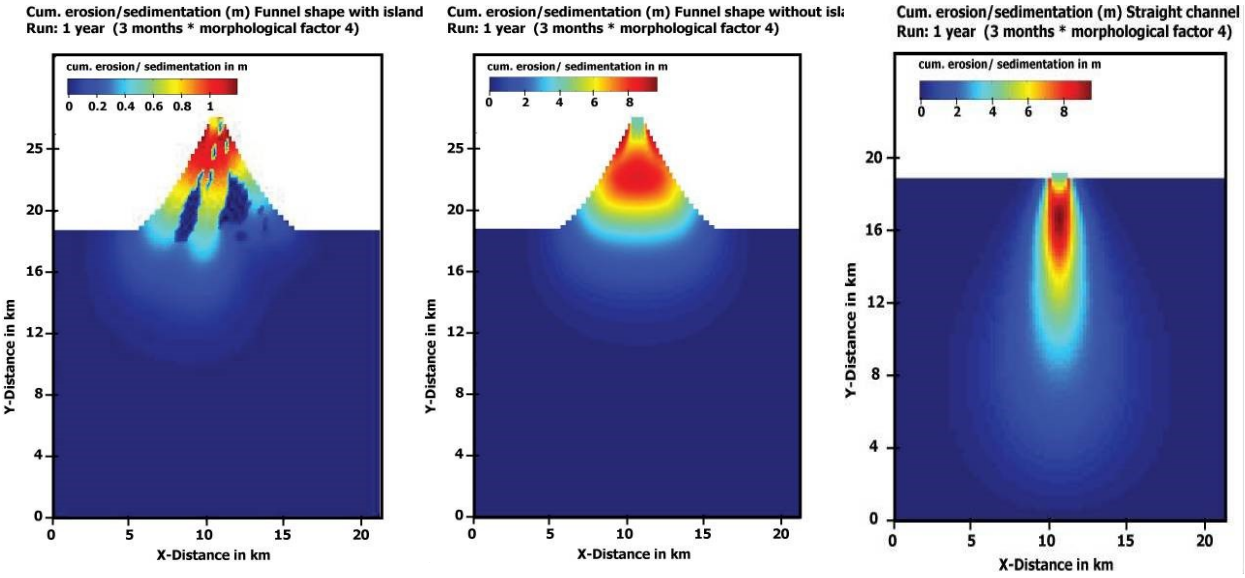


*Figure 6.10 Cumulative erosion/sedimentation (in m/year) for the different morphologies*

The cumulative erosion/sedimentation pattern for the funnel shape with islands *(see Fig. 6.10)* shows the lowest nett sedimentation rate. The local maximum sedimentation is much less (1.2 m/year) than in the funnel shaped grid without islands and the straight channel delta (~8 m/year). The evident difference must be caused by the presence of the islands, which act as an obstacle for flow. The sediment transport has to be divided over three channels, which increases the bed friction and so the initial transport capacity is reduced and bottom sediment is never even being picked up. An additional component is that the tidal influx of sediment is presumably less when the flow velocities are lower.
The sedimentation pattern for the funnel without islands and straight channel both show a similar pattern. The main difference is the width of the delta front. The wide delta front in case of the funnel shape morphology results in a wider spread of the sediment in the prodelta, and thus a more rapid loss of flow momentum *(see Fig. 6.11).*

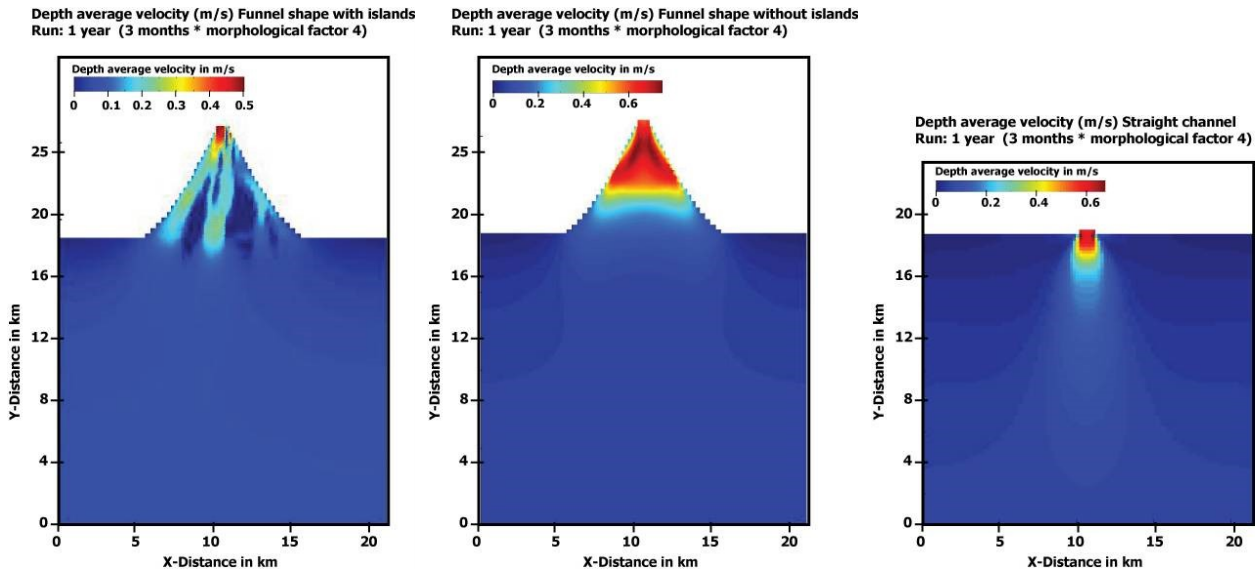


*Figure 6.11 Depth average velocities (m/s) for the different morphologies*

The bed level change in one of the common observation point (33,94) for the different morphologies shows also, that the funnel shape with islands morphology has the lowest sediment accumulation compared to the other two morphologies *(see Fig. 6.12).* This observation point is located near the mouth of the mid-channel (Northern channel).

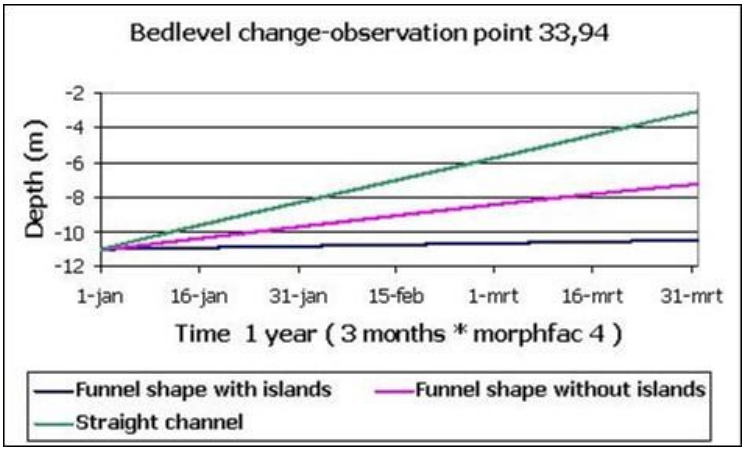


*Figure 6.12 Bedlevel change for different morphologies*

## 6.4 Tide scenarios

Here the base case "intermediate load" scenario has been simulated for one tide, two tides and without tide influences. The goal of simulating this scenario was to study the tidal energy influences on the sedimentation in the distributary channels and the delta area and to distinguish any differences in sedimentation patterns between the one tide, two tides and without tide scenario. The water level as generated for the different tides is shown in *Fig. 6.13.*

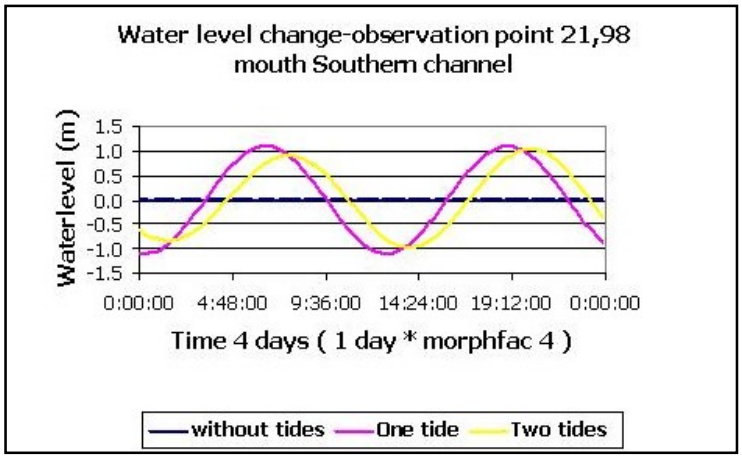


*Figure 6.13 Water level changes due to different tides*

The bedlevel change was observed over approximately one tidal cycle. This was done for all the three distributary channels and hardly any differences in sedimentation rates were observed between one tide, two tides and no tides scenarios for that specific location. The graph with the bedlevel measurements does show different relative channel bottom heights for the one tide, two tides and without tides scenario, whereby the scenario without tides maintains the deepest channel (*Fig. 6.14).* So obviously, the tidal fluxes do affect the nett sedimentation positively.

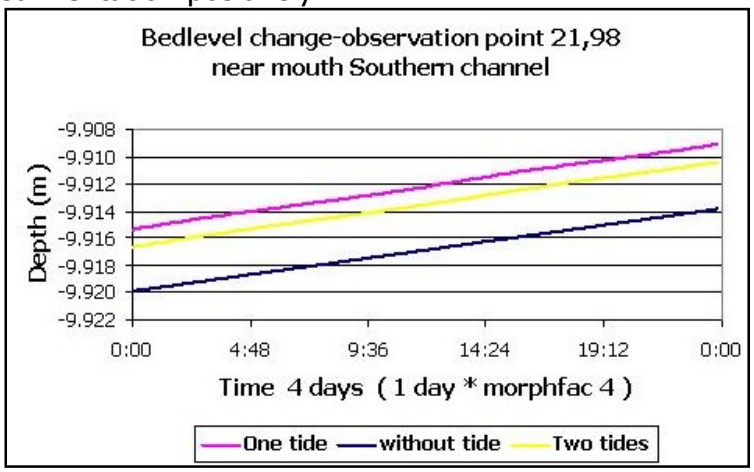


*Figure 6.14 Bedlevel change due to tidal influences at Southern channel*

The grids of sedimentation pattern are shown in *Fig. 6.15.* No significant differences, in sedimentation pattern occur between one- two or without tides scenarios.

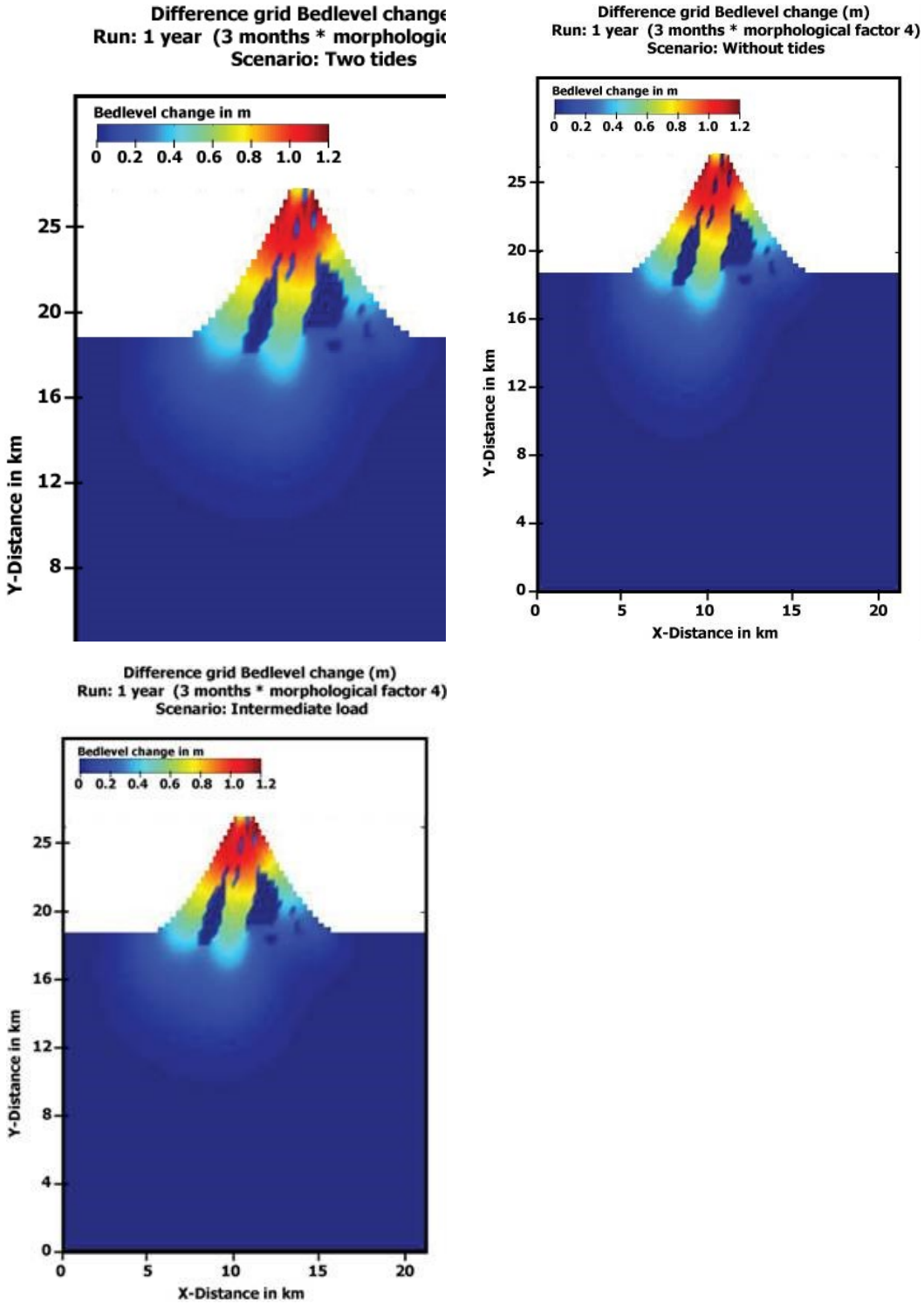


*Figure 6.15 Difference grids bedlevel changes for tide scenarios*

## 6.5 Discharge peak and low flow scenarios

Here the river discharge and sediment load conditions for the base case "intermediate load" scenario were varied to represent high and low river flow conditions. The high flow conditions consist of a 30 % higher river discharge and 50 % higher sediment load, while the low flow condition has a 30 % lower river discharge and 50 % lower sediment load. An additional scenario was simulated in order to investigate sedimentation behaviour in the delta area at extremely low flow, during droughts in El Niño years.

The High –Low flow sedimentation characteristics were compared to the base case "Intermediate load" scenario. The difference grids of the High and Low flow scenario are shown below in *Fig. 6.16.*

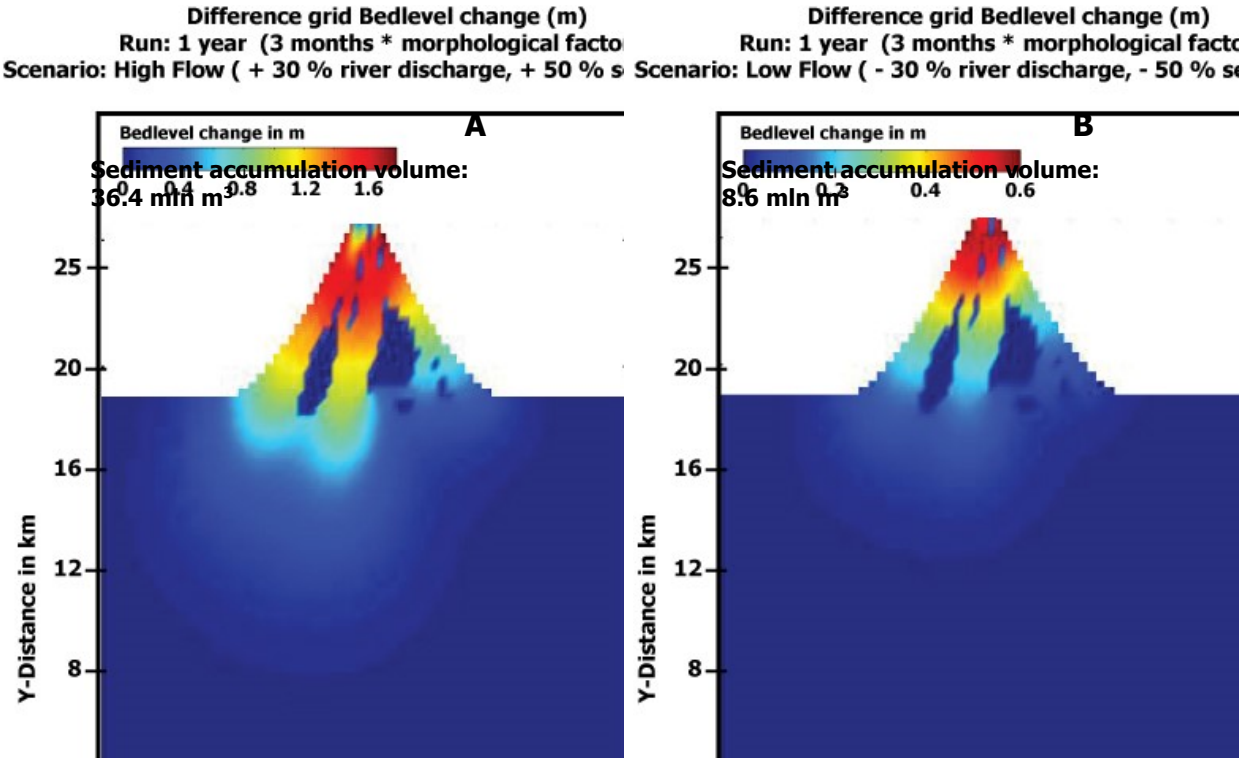


*Figure 6.16 Difference grids High and Low Flow scenario*

The high flow difference grid shows a high amount of sediment which has been deposited in the delta area. This amount of deposit sediment at high flow is 1.6 times larger then the base case sedimentation pattern. The sedimentation during low flow is reduced to one third of the sedimentation value at base case. The low flow scenario has a smaller amount of sediment deposited in the delta area. The high flow- low flow and base case sedimentation relation is shown in *Fig. 6.17.*

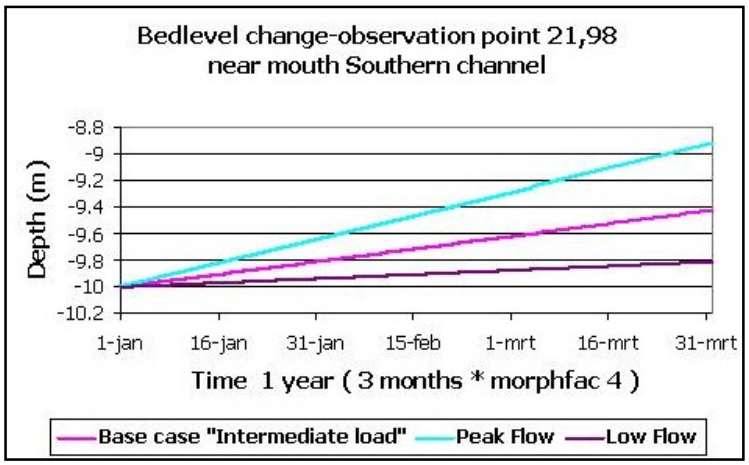


*Figure 6.17 Bedlevel Base case, Peak Flow and Low Flow*

This bedlevel graph for the Base case, Peak flow and Low flow conditions shows that the sedimentation during the peak flow is higher then the base case and the low flow sedimentation is lower then the base case.
The El Niño scenario was simulated to investigate the influences of extreme low flow events, the El Niño, where only the river discharge was lowered from 3500 $m^3$/ s to 1000 $m^3$/ s. The difference of bedlevel change during 1 year simulation of this scenario was made and is shown below in *Fig. 6.18.* Sedimentation seems to be occurred only in the apex area of the delta. Because of the low river discharge and low depth average velocity, sediment transport further downstream was not possible.

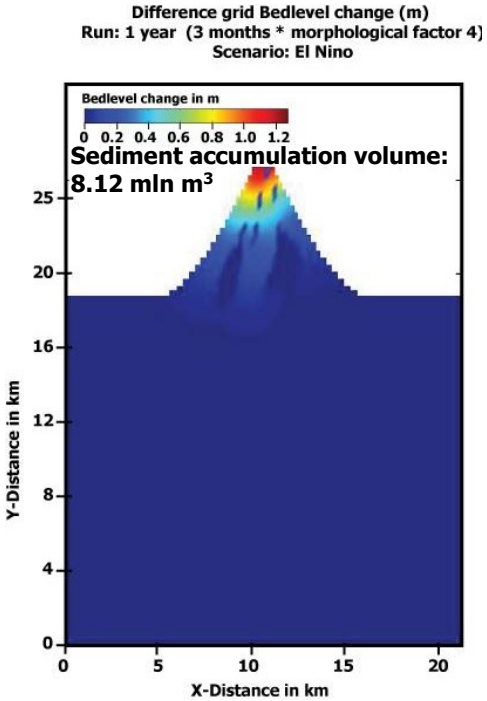


*Figure 6.18 Difference grid bedlevel for El Niño scenario*

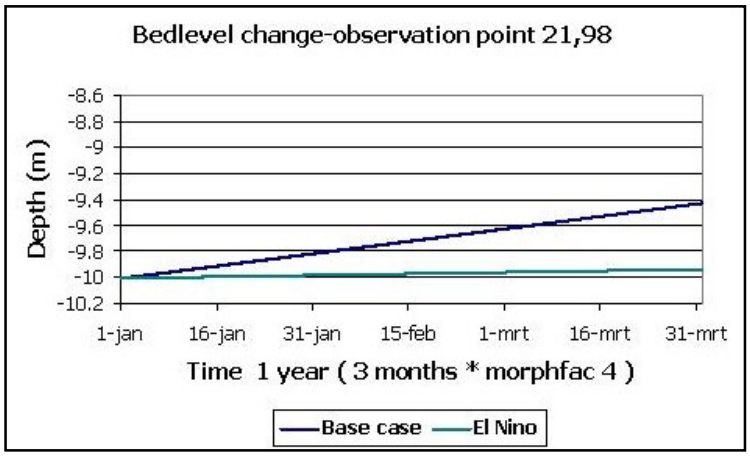


*Figure 6.19 Bedlevel Base case and El Niño scenario*

The bedlevel changes of Base case "intermediate load" scenario is compared with the El Niño bedlevel changes *(see Fig. 6.19).* This has been done for observation point 21, 98 (near mouth Southern channel). It can be observed that there is hardly any bedlevel change for the El Niño scenario. This indicates that no sediment transport toward the delta mouth area has been occurred. At all observation points, the El Niño bedlevel values were below the base case "intermediate load" bedlevel values.

## 6.6 Hydrodynamic scaling scenario

This scenario has as objective to study the hydrodynamic scaling factor that scales the river discharge to the smaller grid while still acknowledging 'normal' hydrodynamic conditions. A comparison with the base case "intermediate load" scenario is made.
The bed level at 6 observation points is compared for both cases (*Fig. 6.5).* It can be clearly observed at all observation points that less sedimentation takes place in case of 75 % scaling factor instead of 50 % related to the "prehuman Syvitski" scenario.

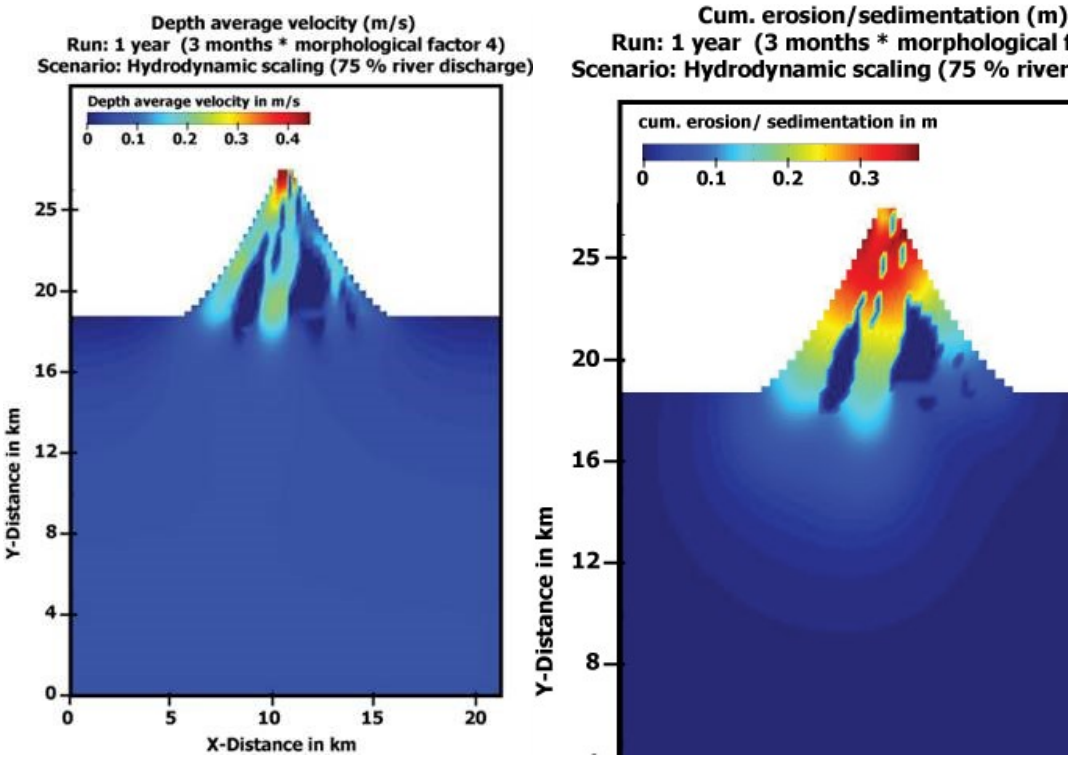


*Figure 6.20 Depth average velocity and cumulative erosion/sedimentation for 75% river discharge*

The depth average velocities as shown above in *Fig. 6.20* are comparable with the Fly delta velocities. The cumulative erosion/sedimentation indicate a maximum sedimentation rate of approximately 35 cm/year. This maximum sedimentation rate is still an overestimation when considering the sedimentation rates reconstructed in the Fly delta area, which do no exceed 10 cm/year. The results of comparing base case ''intermediate load" bedlevel with this scenario shows for all the observation points a lower sedimentation in case of 75 % discharge. The bed level changes during the 75% discharge are compared with the base case "intermediate load" scenario bedlevel. This is shown in *Fig. 6.21.*

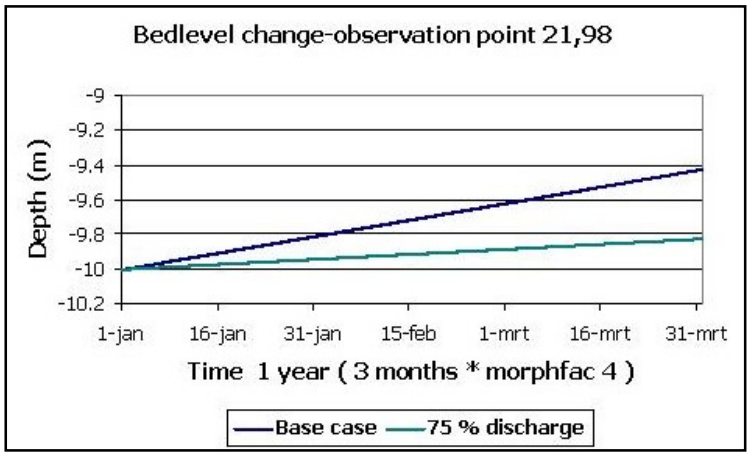


*Figure 6.21 Bedlevel comparison between base case and 75% discharge*

## 6.7 Medium time scale scenarios

To investigate the morphological development on longer term, specifically near a tidal island, a 10 year simulation of the base case "intermediate load scenario" has been executed with tide influence and without tide influences. The general sedimentation of the whole funnel with island area will be shown first by using difference grids. The sedimentation and morphology near a tidal island is discussed in detail by studying the local bed level changes (*Fig. 6.22).*

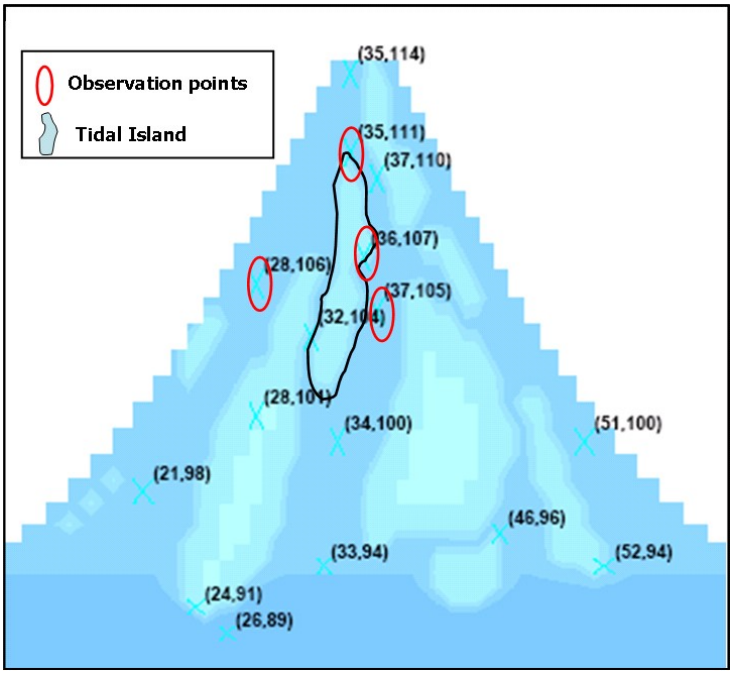


*Figure 6.22 Observation points map for the medium time scale scenario showing the selected island.*

The difference grid maps of the bedlevel changes are shown below in *Fig. 6.23* for 10 year simulation of the base case 'intermediate load" scenario for both the scenario with tidal and without tidal influences.

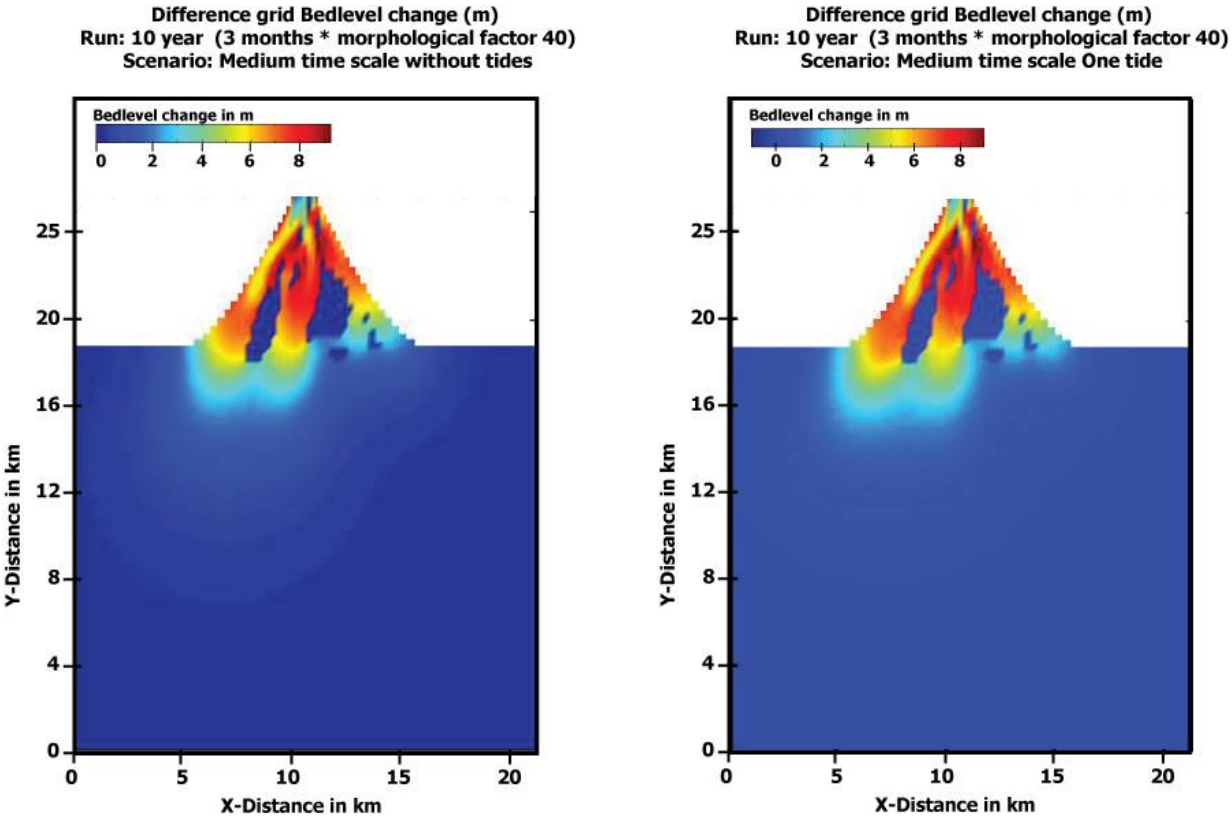


*Figure 6.23 Bedlevel difference grid maps for one tide and without tide influences*

As previously seen in the tidal scenarios there appears little difference in the sedimentation patterns due to the tides. In contrast, when the difference grids of specific grain size components are studied by using the grids of the 'available mass of sand' and 'available mass of clay' significant differences were observed. Especially for the difference grids of the coarser sediment sand *(see Fig. 6.24).*

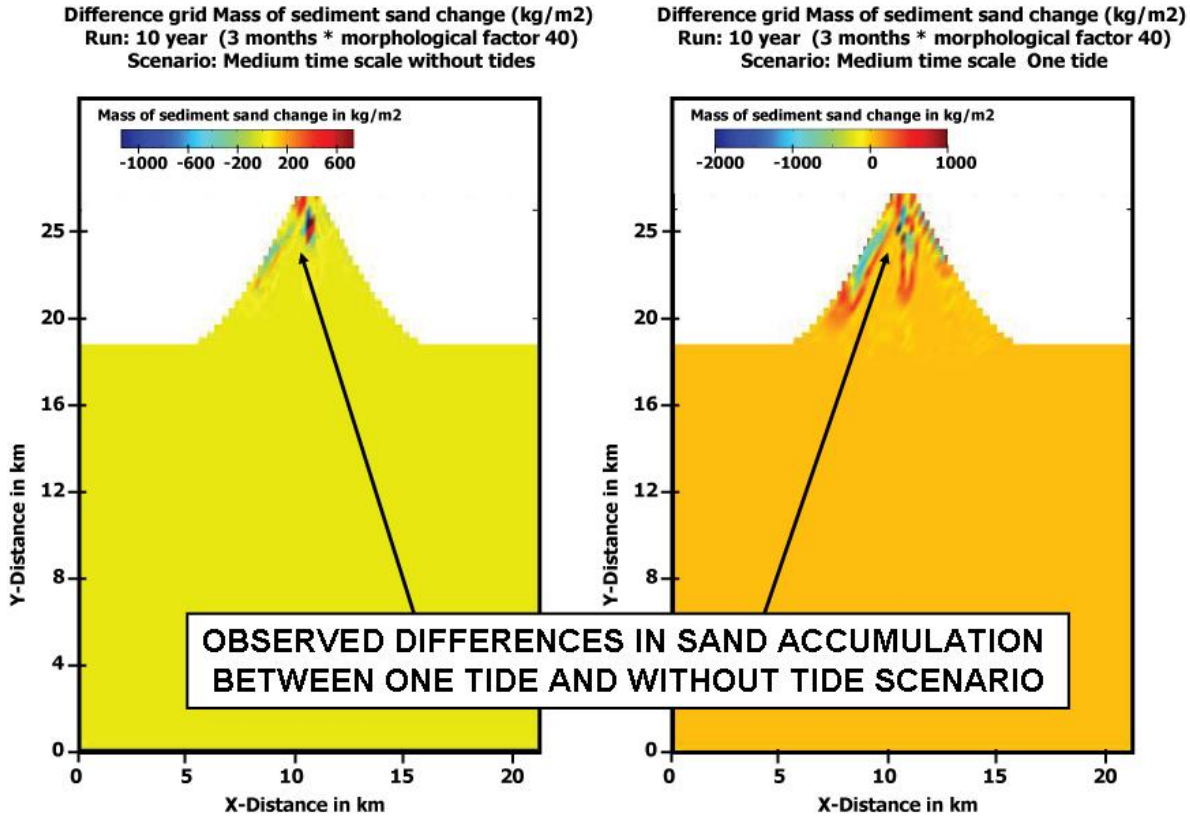


*Figure 6.24 Difference grid for available mass of sand for one tide and without tide influences*

Tides causes only for the available mass of sand a different accumulation pattern when comparing one tide and without tides scenario. The tidal fluxes cause scouring of the two main active channels, even close to the delta apex channel. The morphology of the channel is affected, sands do get scoured in the deeper parts (the negative blue color in *Fig 6.24*), but also deposited along the sides of the channels and on the tidal bars and nearer to the delta front. The grids of the available mass of clay show no differences between the one tide and without tides scenario. This implies that the suspended sediment load transport, i.e the fine-grained clay, is dominated by the fluvial sediment transport.

Data is derived from 4 observation points (*Fig. 6.22)* located at upstream side of the island, at downstream side of the island, in the channel left from the island (Southern channel) and in the channel at the right side (Northern channel).
Again, no significant difference between the bed level changes of one tide and without tide scenarios are reflected in the bed level changes records (*Fig. 6.25).*

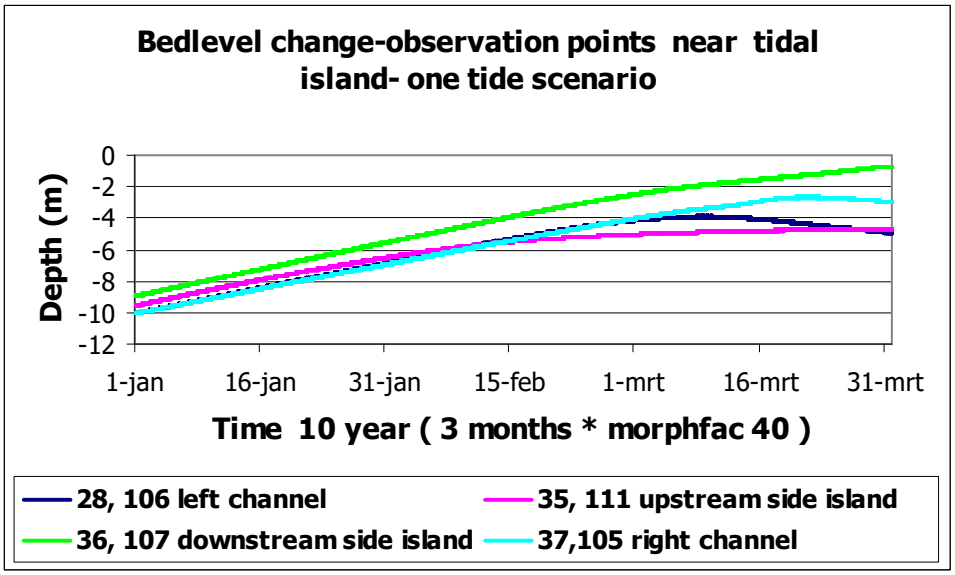


*Figure 6.25 Bed level changes near a tidal island*

The highest amount of sedimentation occurs at the downstream side of the island (observation point 36,107). This may result into growing of the island at the downstream side. The upstream side of the island shows an increase in sedimentation but after some time this is stabilized and no significant bedlevel change occurs at this point any more (observation point 35,111). The right channel (Northern channel) (observation point 37,105) has a period where the bed level increases, after which the bedlevel remain constant and even erosion occurs in the final stages. The left channel observation point (Southern channel) (28,106) shows the same pattern, only the erosional period starts earlier.
The erosion and sedimentation pattern in the channel and near the island is explained as follows. Erosion occurs in the channel left of the island due to tidal influences; at the same time sedimentation caused by tidal influences occurs at the upstream side of the island. This may indicate that the sediment deposited during this period is likely to be carried under tide influenced flow, without tide influences this may not happen.
The cumulative erosion/sedimentation pattern for the upstream and downstream part of the island is shown below in *Fig. 6.26.*

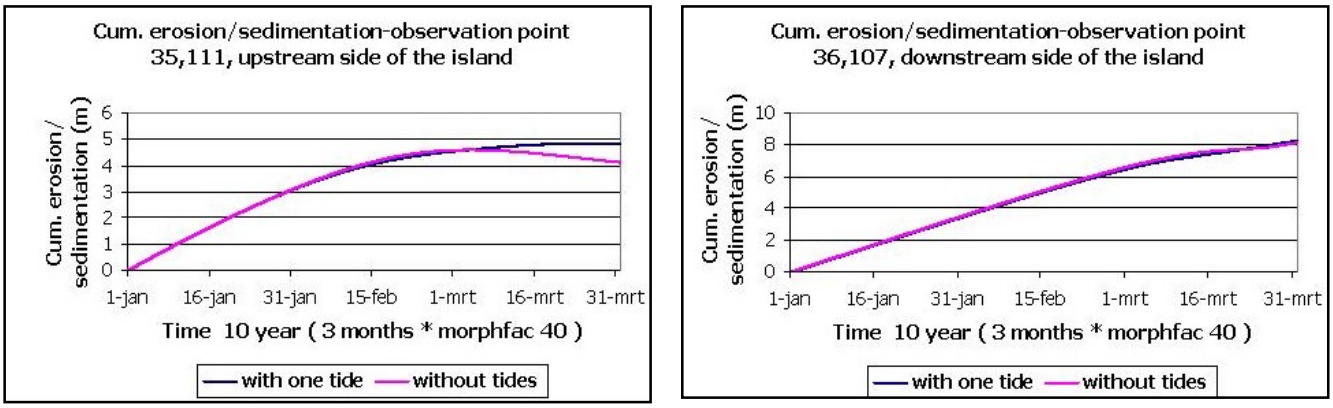


*Figure 6.26 Cumulative erosion/sedimentation near a tidal island*

These graphs indicate that the downstream sides of the islands have a characteristic a pattern of increasing sedimentation, which may cause growing of the tidal island. The upstream side of the island has a gradually increase in sedimentation, but tend to stabilized after a few years. The scenario without tides a clear erosional pattern is shown in *Fig. 6.26.*

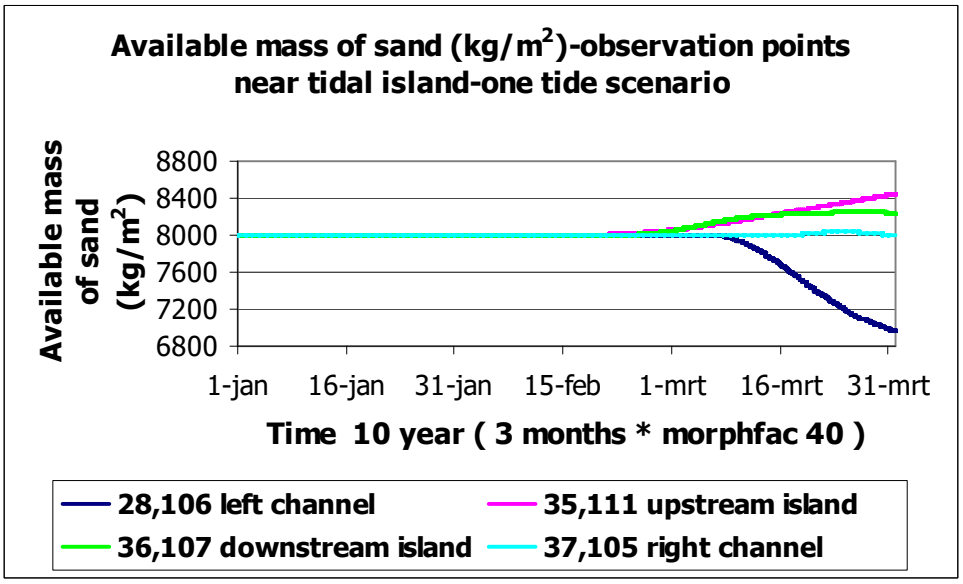


*Figure 6.27 Available mass of sand at observation points near tidal island*

If one studies the different grainsize classes by looking at the 'available mass of sand' graph *(Fig. 6.27),* it clear that the highest sand sedimentation occurs at the upstream side of the island (observation point 35,111). At the downstream side of the island (observation point 36,107) sand accumulation occurs as well. In the right channel (Northern channel) no sand deposition occurs, while in the left

channel (Southern channel) the initial sand layer has been eroded. The high sand deposition on the upstream side of the island supports the idea that tidal influences have a significant role in bedload transport.
The suspended load which consists of clay is the main component causing the high sedimentation at the downstream part of the island. At the upstream part, the lowest clay sedimentation takes place *(see Fig. 6.28).* The right channel (Northern channel) has also a high amount of clay sedimentation, while in the left channel (Southern channel) clay sedimentation increases and after a while it stabilizes itself followed by some erosion.

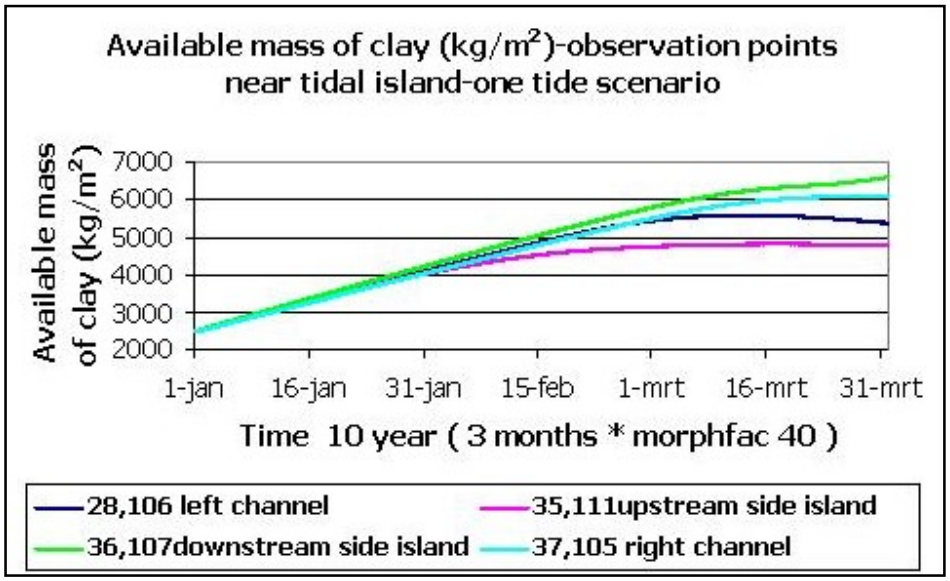


*Figure 6.28 Available mass of clay at observation points near tidal island*

# 7. DISCUSSION AND CONCLUSIONS

## 7.1 Discussion

Modeling of sediment storage and studying the morphological development within the tide dominated Fly delta was the objective of this study. This study has pointed out good strategies to reach this goal.

Considering the Fly delta area as case study, requires modeling values which are an appropriate representation of the Fly delta. This was not so easy, because of the Delft3D model calculations limit the size and resolution of the model grid. It was not feasible to model the entire Fly delta of over 100 by 100 km. The simulation experiments presented, with a grid of ~ 30 by 30 km easily take a day of calculation time to establish a 1 year experiment already. Of course, this downscaling of the delta grid introduces difficulties with scaling the geometry of the channels and the scaling of the river discharge.

The most important Delft3D experiments were designed to study the effect of the different estimates for the total sediment load of the Fly River. The observations and predictions vary by an order of magnitude, from 8 mln tonnes per year to 115 mln tonnes per year.
The depth-averaged velocity values and yearly sedimentation rates were important criteria to judge the output of the simulations for each of the scaled sediment load scenarios. It was found that in our model experiments the flow velocities were generally low. The lowermost discharge scenario, the so-called Syvitski 'prehuman' scenario did result in such low velocities that we disregarded the results. A number of river discharge scenarios showed flow velocities that are within the ranges of the measured flow velocities. It was not possible to achieve sedimentation values equal as for the Fly delta. All scenarios overestimate the observed sedimentation rate, which is only a few centimeters to maximally 10 cm/year. The overestimation may be partly related to the applied scaling in Delft3D, but it is also possible that the observed values for sediment load are too high. The concern about the observations is related to the fact that sediment loads have been measured at Kuambit, more than 300 km upstream from the delta apex. The meandering Fly River has a low-gradient course in the last stretch and may not transport as much sediment as reported.

It was decided to select the scenario called 'intermediate load' for further experiments because the depth-averaged velocity appeared appropriate for the dynamics in the Fly delta channel and the scenario still had the lowest sedimentation rates (between 0-1.2 m/year).
The sedimentation rate at local observation points shows that the bedlevel changes vary within the delta. The highest sedimentation has been observed in the mid-delta area, and the lowest sedimentation rate at the channel mouth.

This suggests that sediment is preferably been deposited and stored in the mid-delta area. Sedimentation is also different for the individual channel or delta distributaries. The differences in sedimentation rates are related to the local depth-averaged velocity in combination with the tidal influences. The transport capacity appeared very low, due to the limited flow velocities and the tidal sediment flux contributes then to the total amount of sediment that is deposited. Higher sedimentation occurs at the mouth of the middle channel (comparable to the Fly Northern channel) relative to the other two channels. This is in contrast to dynamics in the Fly delta, where Wolanski (1993) observed that the Far Northern channel is relatively less active and has high sedimentation rates. We speculate that this may have to do with the orientation of this channel and the dominant trade wind direction, causing an influx of sediments due to wave action. Sofar, waves have not been modeled so the influence can not be evaluated yet.

A number of scenarios have been simulated to evaluate the effect of seasonal differences in river discharge and sediment load. The differences in amount of deposited sediment between the high flow and low flow scenario, shows that the decrease in sediment deposition during low flow was relatively larger. The sedimentation changes to one third of base case sediment deposition. Contrastingly, the increase in sediment deposition under peak flow conditions is relatively less important, sedimentation increases to 1.5 * the base case sediment deposition. For the El Niño scenario, representing major drought conditions it was already predictable that a very low sedimentation will be occur, due to low river discharge. The occurrences of low velocity during this period and as well as low river discharge, shows that due to these parameters, sediment deposition was only concentrated near the apex of the delta.

Differences in general sedimentation for with tide and without tide scenarios are difficult to observe in a one year simulation. We found that the differences do occur, but that they are grainsize specific and influence the specific sediment sand/clay sedimentation pattern. Another option is that these sedimentation differences are only locally present within specific parts of the delta. It may be suggested that morphological changes as for example evolution of tidal bars may occur at longer term runs. The influence of the tidal scenarios on the distribution of coarse-grained sediment transported as bedload could have reservoir geological implications.

Simulations for longer-term create the possibility to study the morphological development within the delta in more detail. Differences between runs are more easily observed when simulations have been executed for longer time period.
At the apex of the delta higher depth- averaged velocities were determined for the simulations while at the delta mouth area lower velocities were modelled. The bed level change is also higher for the apex then for the delta mouth area.

The changes around a specific island show scouring of the channel bottom, especially if a tidal component is modeled. Coarse-grained sediment is simultaneously deposited along the sides of the channel. This sedimentation mechanism has been identified in field studies in the Fly delta by a.o. Walsh et al., 2004. Another pattern that is only observed under the 'one tide' scenario is that the highest sand accumulation has been observed at the upstream part of the island and highest clay accumulation at the downstream part of the island.
This pattern forms an important distinction between more fluvial-dominated deltas and tide-dominated deltas.

## 7.2 Conclusions

The model experiments consistently overestimate sedimentation rates in the delta grid as compared to measured sedimentation rates in the Fly delta. This may be related to model geometry downscaling. Another explanation is that the sediment load measurements high upstream in the Fly River cannot be extrapolated for the Fly delta. The scaling factors have to be considered as an important factor to establish a good calibration of modelled results with real measurements. It is extremely important to build a grid and bathymetry which is appropriate for the applied discharge. The discharge reflecting the width-depth-velocity relation has to be considered as an important way to acknowledge appropriate hydrodynamic flow.

Longer term runs are required to distinguish significant morphological differences for the with tide-two tides and without tides scenario. The largest sedimentation occurs at the downstream side of the tidal island, this may cause growing of this island in downstream direction. Highest sand accumulation has been observed at the upstream part of the island and highest clay accumulation at the downstream part of the island but only under the scenarios that include a tidal component. These patterns form an important distinction between more fluvial-dominated deltas and tide-dominated deltas and may be used in reservoir characterization studies.

Peak flow conditions could enhance morphological changes within the delta area due rapid changes in bedlevel in terms of sedimentation. It is highly likely that under El Nino conditions hardly any sedimentation takes place. The modeled scenario did not show significant channel erosion due to tides at that time. Also the periods that these extreme conditions occur are still rather short to have an erosional effect.

## 7.3 Recommendations

The scaling factor related to the Fly delta, has to be evaluated and modified. This can be properly done if real digital bathymetry data of the Fly delta is achieved. The focus can also be limited to a smaller part of the Fly delta for which enough reliable bathymetric data is available. Except of this, other data measurements such as sediment load, river discharge, velocity and tidal ranges, specifically for this small area has to be available on detail level. This would improve calibration efforts between the modelled results and real measurements.

Longer term runs has to be executed for investigating the significant morphological differences and sediment pattern changes for the with tide-two tides and without tides scenario. The results of these runs could be used for advanced sedimentation pattern studies in terms of tidal bar growth and specifically for sand and clay depositional and erosional patterns. To extrapolate this for the total delta, similar tidal bar growth analyzes has to be done for other tidal bars located at different positions within the delta area.

Validation of modelled sedimentation results with outcrop analogue data is needed. Outcrop analogues studies of similar type of tide dominated deltaic deposits could enhance the interpretation of modelled erosion and sedimentation patterns. At the other side, modelled results should also be tested during reservoir characterization studies in oil reservoirs located within similar tide dominated depositional environments as the Fly delta.

# ACKNOWLEDGEMENTS

I would specially like to thank my direct supervisors Irina Overeem and Joep Storms for their input and care during this project. Further I would like to thank Bas van Maren and Gerben de Boer for their good advices about the modeling part of this research.

I also like to express my thanks to the people of WL/Delft Hydraulics, from whom I always could get the right suggestions about the DELFT3D software. Especially, Jose Haze, Bert Jagers, Lenie van der Poel and Johan Dijkzeul who provides me always with the best advices and literature about Delft3D.

Last but not least, I also like to thank the other committee members Professor Kroonenberg and Gert-Jan Weltje, for their interest and valuable advices at the stage of selecting my MSc research topic.

Thank you all…people whom I mentioned and others whom I forgot to mention for your support, time and everything else….

# REFERENCES

## LITERATURE REFERENCES


1) Ambrose, W.A. and Ferrer, E.R. (1997) Seismic stratigraphy and oil recovery potential of tide-dominated depositional sequences in the Lower Misoa formation (Lower Eocene), LL-652 Area, Lagunillas Field, Lake Maracaibo, Venezuela, Geophysics, Vol. 62, 5, 1483-1495

2) Baker, E.K., Harris, P.T., Keene, J.B. and Short, S.A. (1995) Patterns of sedimentation in the macrotidal Fly River delta, Papua New Guinea. In: Flemming, B.W. and Bartholoma, A. eds. Tidal Signatures in Modern and Ancient Sediments, International Association of Sedimentologists Special Publication, 24, 193-211

3) Bearman, G. (1989) Waves, Tides and Shallow-Water Processes, Pergamon Press, Oxford and New York

4) Dalrymple, R.W., Baker, E.K., Harris, P.T. and Hughes, M.G. (2003) Sedimentology and stratigraphy of a tide-dominated foreland basin delta (Fly river, Papua New Guinea). In: Sidi, F.H., et al, Tropical deltas of Southeast Asia-sedimentology, stratigraphy and petroleum geology. SEPM Special Publication, vol 76, 147-173.

5) Delft 3D Flow, user manual (2005) Simulation of multi-dimensional hydrodynamic flows and transport phenomena, including sediments, WL Delft Hydraulics

6) Dietrich, W.E., Day, G. and Parker, G. (1999) The Fly River, Papua New Guinea; Inferences about River Dynamics, Floodplain Sedimentation and Fate of Sediment. In: Miller, A.J. and Gupta, A. Varieties of Fluvial Form, John Wiley & Sons Ltd, 14, 345-376.

7) Elliot, T. (1986) Deltas. In: Reading, H.G. (ed.), Sedimentary Environments and Facies. Blackwell Science, Oxford, 113-153.

8) Galloway, W.E. (1975) Process framework for describing the morphologic and stratigraphic evolution of deltaic depositional systems. In: Broussard M.L. (ed.), Deltas: Models for Exploration. Houston Geological Society, Houston, 87-98.

9) Galloway, W.E. and Hobday, D.K. (1983) Terrigenous Clastic depositional systems, Springer-Verlag, New York, 5, 81-113; 359-362

10) Gupta, R. and Johnson, H.D. (2001) Characterization of heterolithic deposits using electrofacies analyses in the tide-dominated Lower Jurassic Cook Formation (Gullfaks field, offshore Norway), Petroleum Geoscience, Vol.7, 321-330

11) Hamilton, W. (1979) Tectonics of the Indonesian region, Geological Survey Professional paper 1078, Washington.

12) Harris, P.T., Baker, E.K., Cole, A.R. and Short, S.A. (1993) A preliminary study of sedimentation in the tidally dominated Fly River delta, Gulf of Papua. Continental Shelf Research, 13 (4), 441-472.

13) Harris, P.T., Hughes, M.G., Baker, E.K., Dalyrymple, R.W. and Keene, J.B. (2004) Sediment transport in distributary channels and its export to the pro-deltaic environment in a tidally dominated delta: Fly River, Papua New Guinea. Continental Shelf Research, 24, 2431-2454.

14) Johansen, J.S. and Djamaoeddin, A. (2003) Sequence Stratigraphy of Bangko Field, Sihapas Group (Miocene), Central Sumatra Basin, Indonesia, AAPG Annual Convention, Salt Lake City, Utah

15) Johnson, R.W. (1976) Late Cainozoic Volcanism and plate tectonics at the Southern margin of the Bismarck sea, Papua New Guinea. In: Johnson, R.W. Volcanism in Australasia. Elsevier Scientific Publishing company, Amsterdam, 101-116

16) Lesser, G.R., Roelvink, J.A., van Kester, J.A.T.M. and Stelling, G.S (2004) Development and validation of a three-dimensional morphological model, Coastal Engineering, 51, 883-915

17) Martinius, A.W., Ringrose, P.S., Brostrøm, C., Elfenbein, C., Næss, A. and Ringås, J.E. (2005) Reservoir challenges of heterolithic tidal sandstone reservoirs in the Halten Terrace, mid-Norway, Petroleum Geoscience, vol.11, 3-16

18) Milliman, J.D. (1995) Sediment discharge to the ocean from small mountaineous rivers: the New Guinea example. Geo-Marine Letters, 15, 127-133.

19) Nichols, G. (1999) Sedimentology and stratigraphy, Blackwell Science, UK, 149-166.

20) Parker, G., Akamatsu, Y., Muto, T. and Dietrich, W. (2004) Modeling the effect of rising sea level on river deltas and long profiles of rivers, Proceedings, International Conference on Civil and Environmental Engineering (ICCEE-2004), Hiroshima University, Japan, July 27 to 28, 2004.

21) Reynolds, A.D. (1996) Paralic Successions. In: Emery, D and Myers, K.J. (ed.), Sequence Stratigraphy. Blackwell Science, UK, 134-177.

22) Roelvink, J. A. (2006) Coastal morphodynamic evolution techniques, Coastal Engineering, 53, 277-287

23) Shanmugam, G., Poffenberger, M. and Torro Alava. J (2000) Tide-dominated estuarine facies in the Hollin and Napo ("T" and "U") formations (Cretaceous), Sacha field, Oriente Basin, Equador, AAPG bulletin, vol.84, 5, 652-682

24) Syvitski, J.P.M., Vörösmarty, C.J., Kettner, A.J. and Green, P. (2005) Impact of Humans on the flux of terrestrial sediment to the global coastal ocean, Science, vol 308, 376-380

25) Toha, B. (2000) High resolution sequence stratigraphy of the Minas Oil Field: a key reference for reservoir management and EOR field development, AAPG bulletin, Vol. 84, 9, 1506

26) Van Rijn, L.C. (1983) Principles of sediment transport in rivers, estuaries and coastal seas, Aqua Publications, Amsterdam

27) Walsh, J.P. and Nittrouer, C.A. (2004) Mangrove-bank sedimentation in a mesotidal environment with large sediment supply. Marine Geology 208, 225-248.

28) Wolanski, E., Norro, A. and King, B. (1995a) Water circulation in the Gulf of Papua. Continental Shelf Research, 15, 2-3, 185-212.

29) Wolanski, E. and King, B. (1995b) Dynamics of the turbidity maximum in the Fly River estuary, Papua New Guinea. Estuarine, Coastal and Shelf Research, 40, 321-337.

30) Wolanski, E. and Gibbs, R.J. (1995) Flocculation of suspended sediment in the Fly River estuary, Papua New Guinea. Journal of Coastal research, 11(3), 754-762.

31) Wolanski, E., King, B. and Galloway, D. (1997) Salinity intrusion in the Fly River estuary, Papua New Guinea. Journal of Coastal research, 13(4), 983-994.

INTERNET REFERENCES

http://www.vims.edu/margins
http://rapidfire.sci.gsfc.nasa.gov
http://www.ccreservoirs.com

# LIST OF FIGURES

# LIST OF TABLES